Article

Genesis of the Eastern Adamello Plutons (Northern Italy): Inferences for the Alpine Geodynamics

Alessio Relvini [1],* , **Silvana Martin [1]** , **Bruna B. Carvalho [1]** , **Giacomo Prosser [2]** , **Luca Toffolo [1]** , **Patrizia Macera [3]** and **Omar Bartoli [1]**

1   Dipartimento di Geoscienze, Università di Padova, Via Gradenigo 6, 35131 Padova, Italy;
    silvana.martin@unipd.it (S.M.); bruna.borgescarvalho@unipd.it (B.B.C.); Luca.toffolo@unipd.it (L.T.);
    omar.bartoli@unipd.it (O.B.)
2   Dipartimento di Scienze della Terra, Università della Basilicata, Macchia Romana 1, 85100 Potenza, Italy;
    giacomo.prosser@unibas.it
3   Dipartimento di Scienze della Terra, Università di Pisa, Via S. Maria, 53, 56126 Pisa, Italy;
    patrizia.macera@unipi.it
*   Correspondence: alessio.relvini@studenti.unipd.it

Abstract: The Corno Alto–Monte Ospedale magmatic complex crops out at the eastern border of the Adamello batholith, west of the South Giudicarie Fault (NE Italy). This complex includes tonalites, trondhjemites, granodiorites, granites and diorites exhibiting an unfoliated structure suggesting passive intrusion under extensional-to-transtensional conditions. Major, minor elements, REE and isotopic analyses and geochemical and thermodynamic modelling have been performed to reconstruct the genesis of this complex. Geochemical analyses unravel a marked heterogeneity with a lack of intermediate terms. Samples from different crust sections were considered as possible contaminants of a parental melt, with the European crust of the Serre basement delivering the best fit. The results of the thermodynamic modelling show that crustal melts were produced in the lower crust. Results of the geochemical modelling display how Corno Alto felsic rocks are not reproduced by fractional crystallization nor by partial melting alone: their compositions are intermediate between anatectic melts and melts produced by fractional crystallization. The tectonic scenario which favored the intrusion of this complex was characterized by extensional faults, active in the Southalpine domain during Eocene. This extensional scenario is related to the subduction of the Alpine Tethys in the Eastern Alps starting at Late Cretaceous time.

Keywords: Eocene magmatism; Southern Alps; geodynamics; crustal anatexis; Alpine geology

1. Introduction

Adamello is the largest alpine batholith of Tertiary age (670 km^2 and 3 km of vertical relief) emplaced under extensional-to-transpressional regimes in the Central Southern Alps, after the Europe-Adria collision (Figure 1) [1–3]. Its magmatic activity started about 43 Ma ago (Re di Castello and Corno Alto U-Pb zircon age) and reached its peak during the Late Eocene with a progressive age decrease to 33 Ma towards NE, and a final cooling down to 29 Ma (NE Presanella; Rb-Sr age on Bt and Ms) [4–8]. The oldest plutons are aligned at the southern and southeastern margin of the batholith, close to the South Giudicarie and Val Trompia faults [7].

The Adamello magmatism was continuously sustained over a 10 Ma-long period with major pulses at 43–42, 38–36 and 34–33 Ma [5,7]. The first pulse (43–42 Ma) partially overlaps the time span recorded for the emplacement of magmatic products in the Southern-Southeastern Alps [9–14]. The age of the later magmatic pulses is also consistent with emplacement of dykes and intrusive bodies in the Austroalpine and along the Periadriatic Lineament of Oligocene age [3,15].
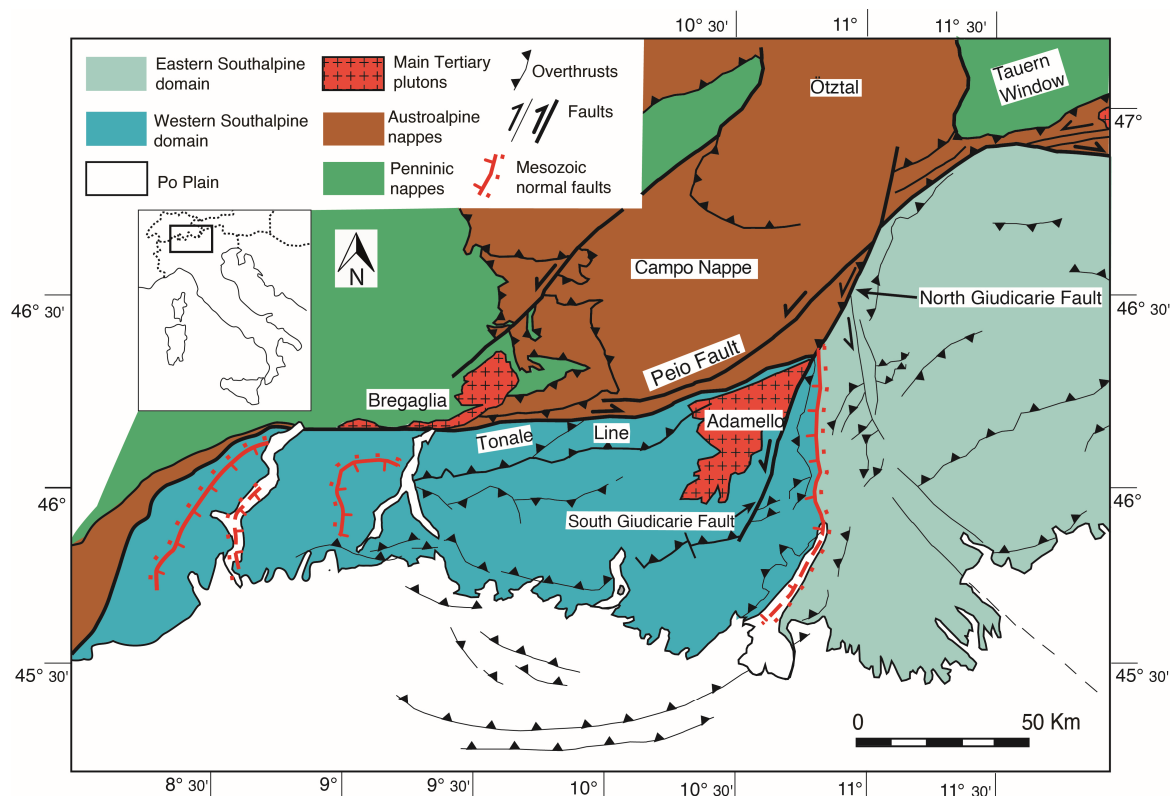
Figure 1. Tectonic map of the Central Alps with main Tertiary plutons.

The Adamello batholith shows a bimodal association of felsic and mafic lithotypes. The former lithotypes are largely more abundant than the latter and consist of plutonic units made up of prevailing tonalite, granodiorite and trondhjemite, while the latter consist of mafic apophyses as well as numerous mafic dykes, surrounding the major plutonic units (Figure 2). While a mantle origin is inferred for the mafic lithotypes, three main hypotheses have been suggested for the genesis of the felsic plutons: (1) fractional crystallization from a picritic basalt [16,17]; (2) magma mixing between mafic and felsic magmas coming from distinct sources, i.e., mantle and lower crust, respectively [18–20]; (3) Assimilation Fractional Crystallization (AFC) of a mantle-derived magma, e.g., either a high-Al basalt or a picritic basalt with crustal material [21–26].

A key area to investigate the origin of felsic rocks from Adamello is the Corno Alto pluton, located on the eastern edge of the batholith, west of the South Giudicarie Fault. It is a composite pluton, comprising trondhjemite, tonalite, granodiorite with granitic portions. Mafic apophyses are present at the border of the main plutons and leucocratic dykes intrude in both the Southalpine basement and the earlier magmatic bodies. Corno Alto rocks are mainly massive, without a clear magmatic foliation. Recent geochronological data highlight that Corno Alto pluton is the oldest in the Adamello framework [7]. In this contribution, the geological setting of Corno Alto, its origin and evolution starting from the intrusion of earlier mafic apophyses and dykes are investigated, also considering the intrusive relationships with the adjacent Central/Western Adamello (ADA) and Re di Castello tonalite plutons (RDC).

We present new geological and geochemical data, on the mafic and felsic rocks of the Corno Alto pluton to investigate its sources and magmatic evolution. Geochemical modeling was also conducted to evaluate both the crystallization of possible parental magmas and the partial melting of Southern Alps upper and lower crust. Finally, we discuss the role of the Giudicarie Fault System in the intrusion forming process.

2. Materials and Methods

2.1. Geological Survey

Geological maps at 1:10,000 scale of the Corno Alto pluton were obtained during mapping of the Tione di Trento and Malé 1:50,000 sheets of the Geological map of Italy (CARG project) [27,28]. A SW–NE trending cross section of the Adamello batholith traced orthogonal to the magmatic contacts from Bazena to Pinzolo illustrates intrusion relationships between plutons, Southalpine basement and sedimentary cover (Figure 2).
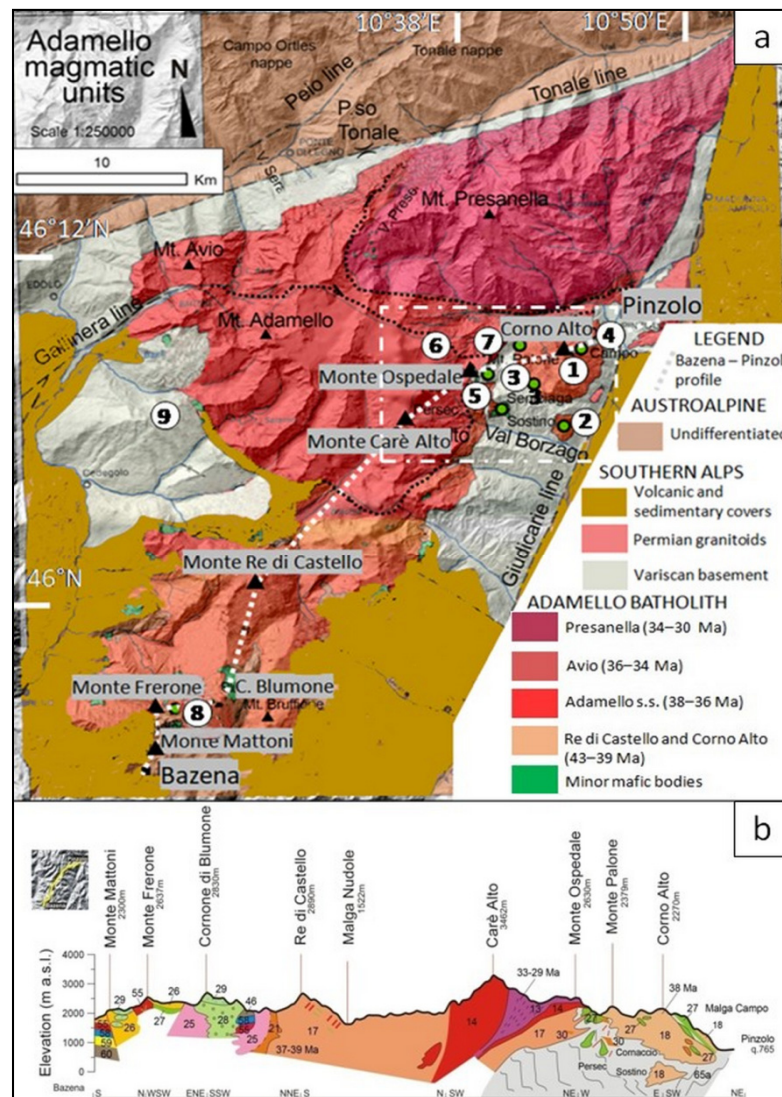
Figure 2. (**a**) Samples locations in the Adamello batholith and trace of the geological section. Numbers as follows: (1) Corno Alto, (2) M.ga Sostino, (3) M. Palone, (4) M.ga Campo, (5) M. Persec, (6) M. Ospedale, (7) M.ga Seniciaga Bassa, (8) Southern Re di Castello (M. Mattoni), (9) M. Marser. (**b**) Bazena–Pinzolo geological section. Legend for the numbers after Callegari et al. [29] 13: Val di Genova tonalite (age 31–30 Ma), 14: Western Adamello tonalite (42–34 age Ma), 17: Re di Castello tonalite (age 37–39 Ma), 18: Corno Alto and Sostino trondhjemite and granite (42–33 Ma), 21: Lago d'Arno-Lago Boazzo granodiorite (41–39 Ma), 25: Lago della Vacca tonalite (43–40 Ma), 26: Val Fredda leucotonalite (42–39 Ma), 27: gabbro and dioritehornblende-rich (41–37 Ma), 28Cornone di Blumone gabbro (42–40 Ma), 29: Stratified gabbro of Monte Mattoni and Cornone di Blumone (42–41), 46: Dolomia Principale, 55: Angolo limestone, 58: Bovegno cargneule, 59: Servino Formation, 60: Upper Permian sandstone and clays, 65: Val Rendena Southalpine basement. Ages after Del Moro et al. [21].

2.2. Petrography, Mineral Chemistry and Geochemistry

A total of 150 samples were collected from different lithologies of the Corno Alto and Monte Ospedale area for the CARG project (sampling sites and related acronyms are reported in Tables 1 and S1, and in Figures S1–S4). Among them, 26 samples have been analyzed and are reported in Table 1. (see Supplementary Material for further information).

Table 1. Corno Alto–Monte Ospedale samples sites, lithologies and mineral associations. Mineral abbreviations after Whitney and Evans [30]. Samples marked by * after Macera et al. [22]. For accurate locations see Table S1, Figures S2 and S3.

Sample	Lithotype	Location	Mineralogy
A77-5 *	Corno Alto trondhjemite (CATr)	Gelada	Pl, Qz, Bt, Ms, Kfs. Acc: Ap, Zrn, Opq
AP2	Corno Alto trondhjemite (CATr)	Corno Alto	Pl, Qz, Bt, Kfs, Ms, Ep. Acc: Ap, Zrn, Rt, Mag.
A2432	Corno Alto trondhjemite (CATr)	Val S. Giuliano	Qz, Kfs, Pl (altered to Ser + Ep), Bt, Ms.
A77-9 *	Corno Alto trondhjemite (CATr)	Corno Alto	Pl, Qz, Bt, Ms. Acc: Ap, Zrn, Opq.
A78-33 *	Corno Alto trondhjemite (CATr)	Gelada	Pl, Qz, Bt, Ms. Acc: Ap, Zrn, Opq.
GZ183	Corno Alto tonalite (CAT)	Corno Alto	Qz, Kfs, Pl and Ms. Acc: Ap, Zrn.
GZ184	Corno Alto tonalite (CAT)	M.ga Campo	Qz, Kfs, Pl and Ms. Acc: Ap, Zrn.
A78-31 *	Sostino granodiorite (SOS)	M.ga Sostino	Qz, Bt, Hbl, Kfs. Acc: All, Tit, Ap, Zrn, Opq.
A77-10 *	Sostino granodiorite (SOS)	M.ga Sostino	Qz, Bt, Hbl, Kfs. Acc: All, Tit, Ap, Zrn, Opq.
AO4 *	Sostino granodiorite (SOS)	M.ga Sostino	Pl, Qz, Kfs, Bt, green Hbl. Acc: All, Tit, Ap, Zrn, Opq.
GZ182	Monte Palone granite (MPG)	M. Palone	Pl, Qz, Ms, Bt. Acc: Chl, Prh, Ap, Zrn, Ilm.
GZ181	Monte Palone granite (MPG)	M. Cornaccio	Pl, Qz, Ms, Bt. Acc: Chl, Prh, Ap, Zrn, Ilm.
A2638	Malga Campo diorite (MCD)	M.ga Campo	Pl, Hbl, Bt. Acc: Opq, Tit, Ep.
A2639	Malga Campo diorite (MCD)	M.ga Campo	Pl, Hbl, Bt. Acc: Opq, Tit, Ep.
AP6	Malga Campo diorite (MCD)	Caladino	Hbl, Pl, Bt, Qz, Kfs; Acc: Ep, Tit, Opq.
A3355	Malga Persec diorite (MPD)	M.ga Persec	Hbl, Act, Pl, Bt, Pl, Qz. Acc: Tit, Ap, Rt, Aln.
A3356	Malga Persec diorite (MPD)	M.ga Persec	Hbl, Act, Pl, Qz, Kf. Acc: Ilm, Tit, Ap, Aln, Ep, Chl, Ms.
A3357	Monte Ospedale diorite (MOD)	M. Ospedale	Pl, Hbl, Bt, Qz. Acc: Ilm, Opq, Ap, Ep, Ms.
A3358	Monte Ospedale diorite (MOD)	M. Ospedale	Hbl, Pl, Bt, Qz. Acc: Tit, Ilm, Ap, Zrn, Py, Ep, Ms.
MK6	Monte Ospedale diorite (MOD)	Val Seniciaga	Hbl, Pl, Bt, Qz, Kfs. Acc: Tit, Ap, Ep, Zrn.
MK9	Monte Ospedale diorite (MOD)	Val Seniciaga	Hbl, Pl, Bt, Qz. Acc: Ap, Ep, Tit, Zrn, Ms.
VF109	Monte Ospedale diorite (MOD)	P.so Altar	Hbl, Pl (altered to Ep + Ms), Bt, Chl, Tit, Ilm.
VF151	Monte Ospedale diorite (MOD)	M. Ospedale	Hbl, Pl, Bt, Qz. Acc: Ilm, Opq, Rt, Ap, Ep, Ms.
VF164	Monte Ospedale diorite (MOD)	M. Ospedale	Hbl, Pl, Bt, Qz, Kfs. Acc: Tit, Opq, Ep, Ms.
MK4	Malga Seniciaga bassa diorite (MSB)	Val Seniciaga	Pl, Hbl, Bt, Qz, Kfs. Acc: Ap, Ep, Tit, Opq.
VF102	Malga Seniciaga bassa diorite (MSB)	M. Cornaccio	Pl, Hbl, Bt. Acc: Opq, Tit, Ep.

2.3. Modelling

In order to understand the origin of the rocks from the Corno Alto–Monte Ospedale area characterized by a large variation in composition, we have performed geochemical modelling of the fractional crystallization and partial melting using two approaches described below.

Fractional crystallization and evolution of an initial mafic magma was simulated on four possible parental magmas selected from the literature: samples JM157 [31], U237 [16] and our own samples MK6–Monte Ospedale diorite; A3355–Malga Persec diorite. We used the software Rhyolite-Melts v 1.2.0 (ETH Zürich, Zürich, Switzerland) which is optimal for

mafic and alkalic melts [32,33]. Simulations were made considering the Quartz–Fayalite–Magnetite (QFM) buffer, at constant pressure of 4 kbar, and 4 wt.% H_2O. The choice of 4 kbar was based on the results of Al-in Hbl geobarometer in Hbl-bearing rocks from the Monte Ospedale diorite. Results of the model can be found in supplementary material (Tables S5–S8). 4 wt.% of H_2O was chosenas this is the minimum amount of H_2O that stabilizes amphibole in the model.

Thermodynamic calculations were performed using Perple_X software (a software generating equilibrium phase diagrams using Gibbs energy minimization procedures) [34], with the internally consistent data set of Holland and Powell [35], in a ten-component $MnO–Na_2O–CaO–K_2O–FeO–MgO–Al_2O_3–SiO_2–H_2O–TiO_2$ (MnNCKFMASHT) system for samples derived from European intermediate crust (ELC1; [36]) and from Adria upper crust (CMP; [37]) and in the eleven component $MnO–Na_2O–CaO–K_2O–FeO–MgO–Al_2O_3–SiO_2–H_2O–TiO_2–O$ (MnNCKFMASHTO) system for rocks derived from European lower crust (ELC2; [36]) and Adriatic crusts (ALC4; [38]), respectively. The following a-x relations were selected for ELC1 and CMP: melt, Grt, Opx, Ms, Bt, Crd and Mag from White et al. [39,40], Ilm from White et al. [41], Pl and Kfs from Holland and Powell [42]. The following a–x relations were instead selected for ELC2 and ALC4: Grt and Opx from White et al. [39,40], Pl from Holland and Powell [42], melt, Cpx and amphibole from Green et al. [43]. Pure phases included Qz, Rt, Ky, Sil and aqueous fluid. All mineral abbreviations after Whitney and Evans [30]. The results of the model can be found in Section 4.2.

3. Geological Setting

The Adamello batholith is emplaced within the corner formed by the South Giudicarie Fault and the Periadriatic Lineament (Figure 2a). It shows a northeastward elongation in contrast with other Periadriatic intrusions that are aligned along the E-striking Periadriatic Lineament (Figure 1). Only Presanella and Avio plutons, forming the northern edge of the batholith, follow the general trend of the Periadriatic Lineament. The whole Adamello batholith is generally assumed as part of the "Magmatic Periadriatic System" [44,45] whose magma is fed by a source region located at the base of the crust and was emplaced parallel to the axis of the Alpine chain, mainly during Oligocene [3,46]. Differently from the "Magmatic Periadriatic System", the Re di Castello and Corno Alto plutons, were emplaced along a NE–SW Giudicarie trend during Eocene, in a time interval spanning from 43.47 ± 0.16 to 39.1 ± 0.3 Ma (U/Pb ages on zircon by Schaltegger et al. [7]). These plutons show no relations with the Periadriatic Lineament, as they are aligned along a SW–NE trend nearly parallel to the Giudicarie Fault System. This latter structure is divided into a northern segment (North Giudicarie Fault), representing the major NE-striking bend of the Periadriatic Lineament, and the South Giudicarie Fault, forming a NE-striking steeply dipping fault zone, representing the most important transverse zone in the nearly E-striking Southalpine thrust and fold belt [47,48].

The South Giudicarie Fault derives from multiple reactivations of a pre-existing fault system present since Permian times as en-échelon grabens [49]. Subsequently, during the Late Triassic to Cretaceous times, a N-striking normal fault system reactivated the same weakness zone. Normal faults were responsible for intense subsidence, connected to the opening of the Lombardian basin in the Western Southalpine Domain (Figure 1), which is separated from the Trento Platform, in the Eastern Southalpine Domain by the N-striking Ballino line [50,51]. Further extensional activity during the Late Cretaceous time has been reported along this fault system [52,53].

During Eocene wide areas of the Southern Alps were affected by intermediate to mafic magmatism. In the central southern Alps, this is indicated by the presence of basaltic, Qz-andesitic, dacitic and rhyodacitic dykes emplaced during the Lutetian–Bartonian time interval (U/Pb zircon ages of 42.1 ± 1 and 39 ± 1 Ma), along E- to NE-trending normal faults [11]. Moreover, several mafic dykes and apophyses intruded bothSouthalpine basement and Permo–Triassic sedimentary cover in Val Rendena, E of the present-day South Giudicarie Fault [13]. Evidence of coeval volcanism is outlined by the presence

of volcaniclastic rocks with a basaltic composition in Early to Middle-Eocene deep-sea sediments exposed along a Giudicarie trend, from Val di Non to the north to Lake Garda to the south [13].Emplacement of Cenozoic intrusive rocks is also observed along the North Giudicarie Fault, as indicated by tonalites and gabbros of Eocene to Oligocene age, sliced along the fault zone [54,55].

The Corno Alto massif consists of a trondhjemite-to-tonalite main pluton (CaTr/CAT; Figures 3 and 4), the granite dyke set of Monte Palone (MPG), Malga Sostino granitoid (SOS), the diorite bodies of Malga Campo (MCD), the gabbro and diorite bodies of Malga Persec (MPD), the Monte Ospedale diorite apophyses (MOD) and late granite dykes (MOG) intruded in the Southalpine basement [29,56–58]. The basement is a pelitic-psammitic sequence, mostly consisting of paragneiss, St ± Grt ± micaschists, Qz-rich schists and orthogneisses with Variscan metamorphism and intruded by Permian granitoids (Figure 4) [59–65].
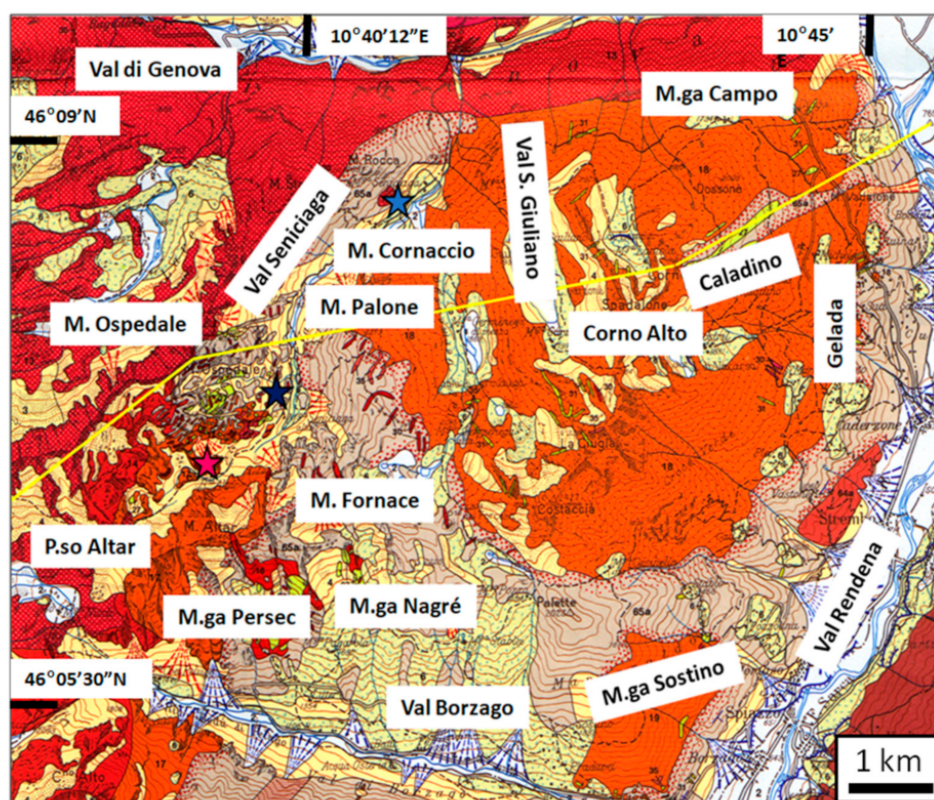

Figure 3. Detailed view of the Corno Alto-M. Ospedale area (framed in Figure 2a), after [29]. Profile trace is in yellow; blue star (Malga Seniciaga bassa, MSB, Table 1), violet star (Malga Seniciaga alta) pink star (Baito Altar).

Variscan basement rocks in Val Seniciaga and Val Borzago record St and Grt in the micaschists indicating transition to ametamorphic grade higher than the one recorded in Val Rendena ([62,65]) (Figure 4). The paragneisses show segregation of Qz in the core of folds and lenses (Figure 5a); layers of Pl (oligoclase, An_{27}) and boudinage along S_2 (Figure 5b). The regional schistosity (S_2) is NE-SW striking in Val Borzago changing to NNE- SSW in Val Seniciaga (Figure S5) [61,62,66]. The intrusion of Corno Alto granitoids, ADA tonalites and of the mafic bodies produced contact metamorphism and parageneses including Bt, Grt, And, Crd, Sil, Kfs and Sp (Figure 5c). And is observed near the diorite dykes of M.ga Campo. Sil, And, Pl (An_{30}) and Crd occur around the gabbro-diorite intrusions of Val Borzago where a temperature of 650–670 °C and a shallow depth of 4–8 km was estimated [65]. At the contact with M. Ospedale diorite, mineral assemblages containing Bt ± And ± Kfs and Grt − And − Sil ± Crd ± Kfs ± Sp are also observed [61,62]. These

field observations highlight how part of the basement, in contact with Corno Alto, was partially melted, producing migmatite-like structure when CAT/CATr intruded.
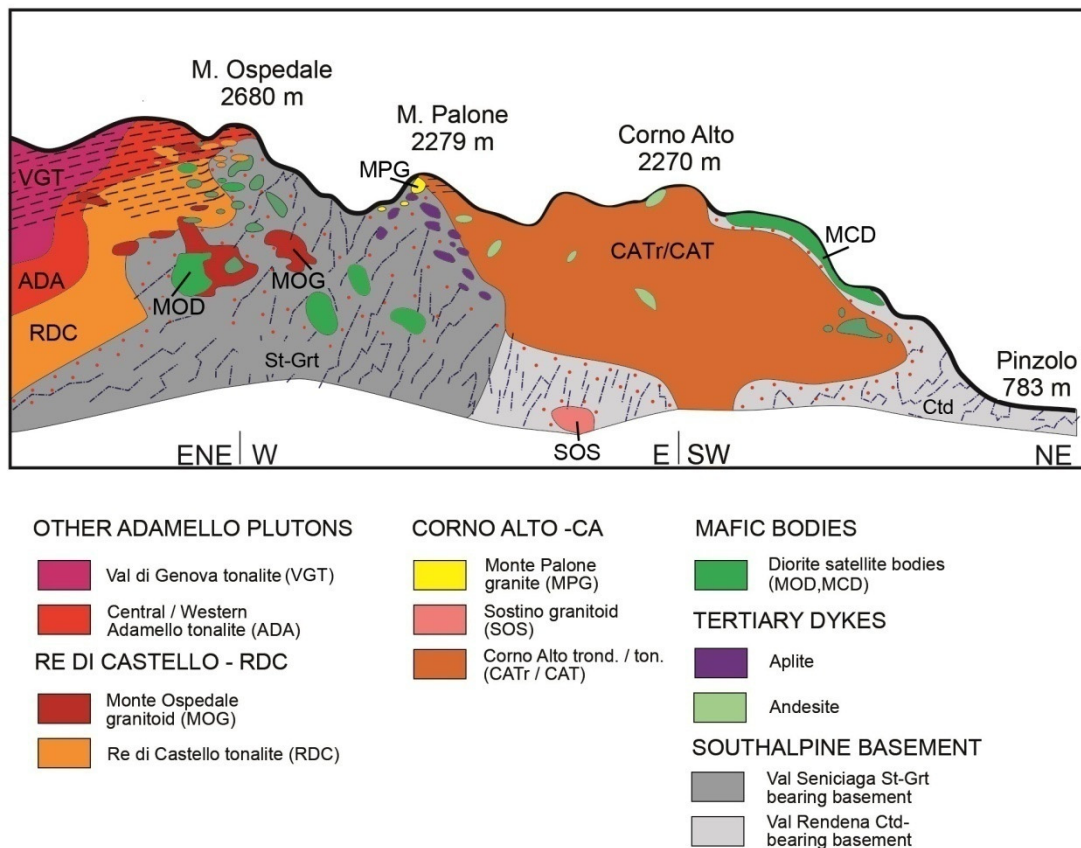

Figure 4. Geological section across Corno Alto–M. Ospedale. Intrusive relationships between diorite apophyses and dykes (green colour), RDC foliated leuco-tonalite (orange), Central/Western Adamello ADA (red), Val di Genova tonalite (violet) and leucogranites (dark red). Straight dashed lines indicate tectonic foliation, purple dashed lines indicate Variscan basement schistosity and red dots identify contact metamorphism. Profile trace is shown in Figure 3.

3.1. Corno Alto Main Body and Felsic Apophyses (CAT, CATr, MPG, SOS)

The Corno Alto pluton is a 20 km^2 sized, rounded, bowl-shaped body located between Val Rendena to the east and Val Borzago to the south, from an altitude of 700 m up to 2427 m (Figures 3 and 4). The schistosity of the wall rocks dips towards the internal part of the pluton becoming subvertical approaching the intrusive contact. Schists were thermally fractured and permeated by melts in a stoping-like process [67]. The pluton includes a granitic core and multiple rims though no sharp limits were recognized in the field by Trener [57] and Salomon [68]. The core, corresponding to the area surrounding Corno Alto peak, is characterized by coarse, hetero-granular rocks, showing no magmatic anisotropy, with Pl (45–50%), Qz (40–35%), Kfs (7–10%), Bt (>3%) Ms (<1%) and Ap, Op, Zrc as accessories (Figure 6a,b). This was defined as a granite by Bianchi and Dal Piaz [69] and successively as a trondhjemite (CATr) on the basis of the chemical composition [8]. The nucleus gradually changes into a tonalite (CAT) as observed towards the Val di Genova [69–71]; near Val di Genova, CAT show evidence of tectonically induced sub-solidus recrystallization [71] (Figure 6c). A granitoid with porphyric structure crops out in the northwestern side of the massif at M. Cornaccio and on the eastern side, in Val Rendena [71,72]. Here, this granitoid contains dismembered fragments of the diorite dykes of M.ga Campo (MCD) (Figure 6d). Other satellite bodies around the main pluton are the apophyses of M.ga Sostino (SOS) and M. Fornace (Figure 3). At M. Palone, a 150 m thick foliated fine-grained

dyke (MPG) is cut by numerous late centimeter-thick aplite dykes. MPG outcrops are sporadic and discontinuous; the granitic dyke embed numerous flattened xenoliths of Variscan basement, generally showing a preferential orientation. The peripheral magmatic body of M.ga Sostino (SOS) consists of granodioritic rocks, resembling CAT in both texture and mineralogy. Recent zircon dating of Corno Alto granitoids yield 43.5–43.2 Ma ages [7]; cooling ages vary from 41–42 Ma (Rb-Sr on Ms) to 33–35 Ma (Rb-Sr on Bt) [1,21,73]. An emplacement pressure of 3.5–4 kbar for the Corno Alto pluton has been proposed based on apatite fission track data in the hypothesis of a "normal" geothermal gradient of 30 °C/km and furtherestimates of the stratigraphic thickness of the overlying Paleozoic and Mesozoic sequence [63,71].
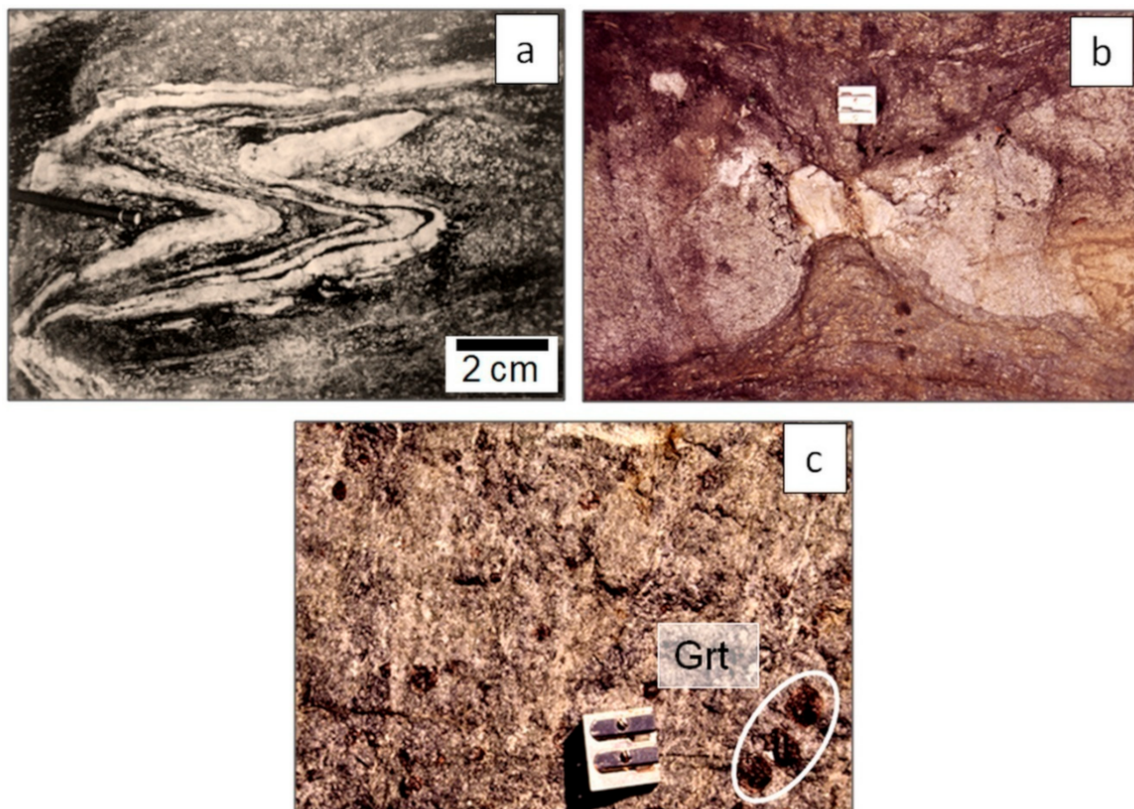
Figure 5. (**a**) Qz-rich folded veinlets, Val Seniciaga basement. (**b**) Boudinage structure in a feldspars-rich layer, Val Seniciaga basement: (**c**) Grt-bearing rock (inside the oval) at the contact with M. Ospedale, upper Val Seniciaga.

3.2. Malga Campo–Caladino Mafic Bodies (MCD)

Mafic bodies crop out on the eastern–northeastern border of the Corno Alto pluton (Figures 3 and 4). The main body is a 100 m-wide dyke, with a ENE-WSW orientation, within a basement slice located south of M.ga Campo. Other minor MCD bodies display a similar E-W to NE-SW orientation. The bodies near Gelada are dismembered by successive CAT intrusions; (Figures 3 and S7). The diorite dyke of M.ga Campo includes Hbl clusters characterized by a preferred orientation parallel to the dyke margin. MCD mineralogical content comprises: Pl (35–45%), Hbl (40–30%) Bt (10–15%), Qz (10–5%) Ep (<5%) Tit (<2%) and secondary Chl. Often, these diorites show fluidal texture with preferred orientation of Pl and Hbl [74]. The enclaves are composed of dominant green Hbl and Pl (zoned labradorite to andesine), Qz, Bt with Mag, Ilm and Tit as accessory and Ep as secondary minerals. Pl phenocrysts are subhedral and zoned (core An_{60} and rim An_{30}), often displaying oscillatory zoning (Figure 6a). Hbl occurs as phenocrysts, often twinned, patchy and poikilitic (including Pl), usually with corroded borders (Figure 6d). Though no absolute

ages are available for MCD, on the base of crosscutting relations, the latter seems to predate CAT/CATr intrusion [71] (Figure S7).
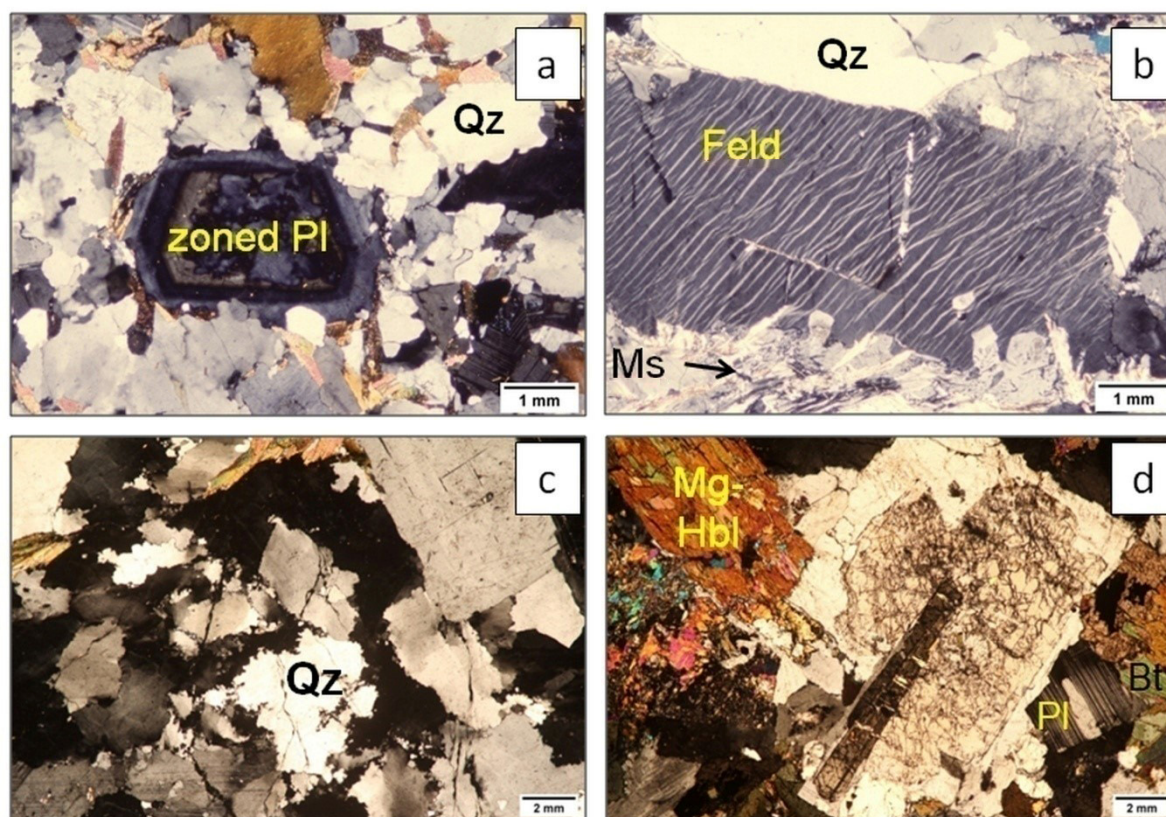

Figure 6. (**a**) Cross polarized light (XPL) image of a zoned plagioclase (Pl) from CATr (sample AP2). (**b**) XPL feldspar porphyroclast containing flame perthites in a quartz + muscovite (Qz + Ms) bearing groundmass (sample A2432). (**c**) XPL image of a recrystallized quartz in tectonically deformed granodiorite at the northern border of Corno Alto (sample A2432). (**d**) XPL image of a zoned plagioclase (Pl) porphyroblast in contact with hornblende (Mg-Hbl) and biotite (Bt) from MCD (sample A2638).

3.3. Val Borzago Mafic Bodies (MPD)

Close to P.so Altar, in the upper Val Borzago, within St-Grt-bearing schists, other mafic bodies occur at M.ga Persec and M.ga Nagrè (names after Figure 3).They were dismembered by the intrusion of Re di Castello (RDC) tonalite and M. Ospedale (MOG) granitoids. Two different rocktypes were observed in the field near M.ga Persec (MPD): a coarse grained granular gabbroid rock, composed of large euhedral Hbl crystals and interstitial Pl, defined as Hbl-gabbro by Bellieni et al. [75], and a fine-grained mafic rock, composed of Hbl, Bt and minor Pl with Mag, Ilm and sphene as accessory minerals. MPD mineralogy is made up of Pl (35–45%), Hbl (45–35%) Bt (15–10%), and Qz (5–10%). Hbl is usually zoned, going from Tschermakite core to Mg-Hbl rim with outer thin rims of actinolitic Hbl [75] (Figure S8). Qz-Bt aggregates seem to postdate crystallization of euhedral Hblwhile minor anhedral Qzappears as an interstitial phase.

3.4. Monte Ospedale Mafic Bodies (MOD, MSB)

M. Ospedale diorites and mafic dykes (MOD) intruded within the Variscan basement of the upper Val Seniciaga between M. Ospedale and M. Cornaccio ridges, following a NE-SW trend (Figure 3). The northeasternmost mafic body of this series crops out between M.ga Seniciaga bassa and M. Cornaccio (MSB, size 0.1 km^2, Figure 3). The main MOD body (0.3 km^2) crops out along the southern slope of M. Ospedale (Figure S6). This bodyconsists

of layers of dominant Hbl interbedded with layers of dominant Pl, showing granular coarse-grained texture exhibiting an isotropic magmatic fabric. Minor MOD and MSB outcrops consist of fine (<1 mm) to coarse-grained crystal (>5 mm). The mineralogical composition includes: Pl (30–50%), Hbl (40–20%) Bt (20–30%), Qz (5–10%), Tit + Ilm (<5%). Pl is either homogeneous or zoned (An_{80-90} cores and An_{30-40} rims). Other mafic bodies crop out along the ridge between M. Ospedale and Baito Altar in the upper Val Seniciaga and at P.so Altar, where diorite is wrapped by RDC tonalite. All the M. Ospedale mafic bodies (MOD) have been heavily dismembered by successive intrusions of RDC and ADA and finally by MOG (Figure S6). The contact rocks show centimeter-sized Grt, And, Sil and Sp (Figure 7d). Between M. Cornaccio and Val Seniciaga, another mafic body appears (MSB), dismembered by CAT [61,62].
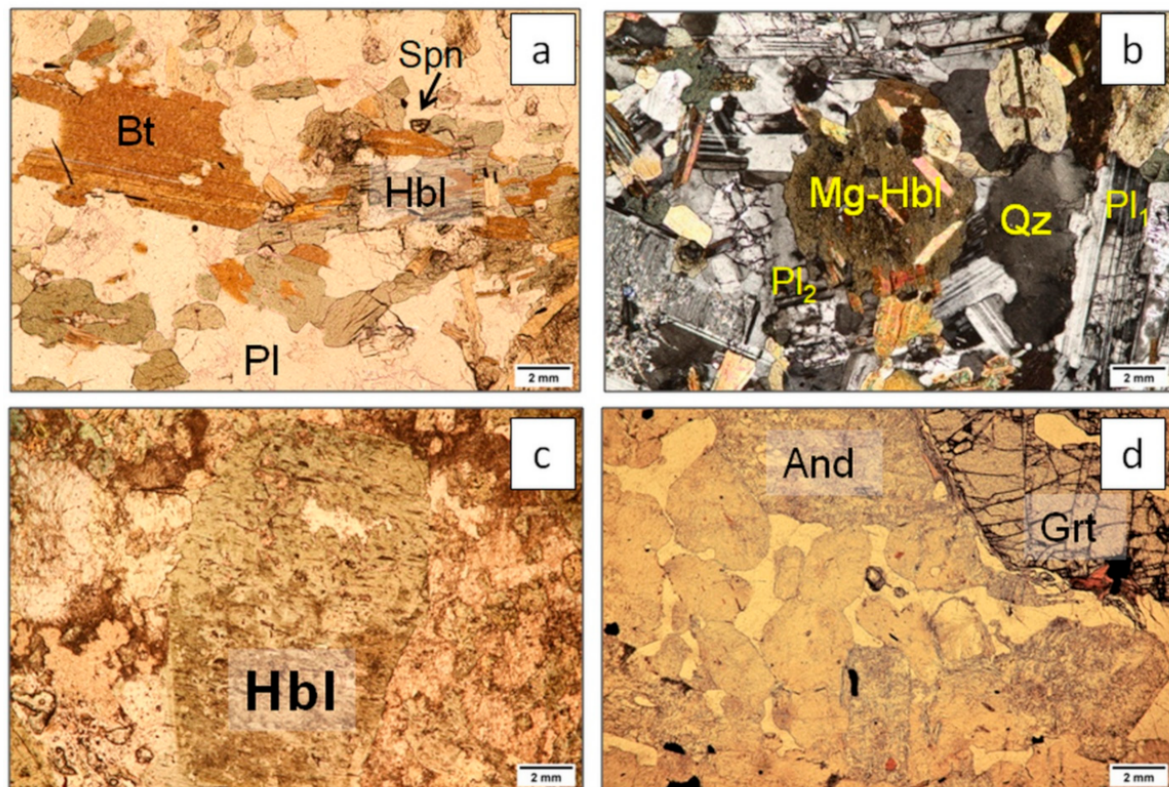
Figure 7. (**a**) Plane polarized light (PPL) image of green hornblende (Mg-Hbl), biotite (Bt) and sphene (Spn) in the plagioclase groundmass of MOD (sample A3357) (**b**) XPL image displaying two generations of plagioclase (euhedral phenocrysts, Pl_1 and subhedral to anhedral crystals Pl_2) in MOD (sample A3357). (**c**) PPL image of a hornblende phenocrystal (Hbl) from coarse grained MPD (sample A3355). (**d**) PPL image of M. Ospedale contact rock with garnet (Grt) and andalusite (And).

3.5. M. Ospedale Felsic Bodies (RDC, ADA, MOG)

In the upper Val Seniciaga, from P.so Altar to M. Ospedale, RDC tonalite is the dominant lithotype. This is a medium-to-fine grained leuco-tonalite, with abundant elongated microdiorite enclaves. Mineral and grainsize variations are very frequently associated withthe repeated alternation of leucocratic and melanocratic lithotypes [69]. The basement shows thermal overprint with mineral associations such as Sil + And or Grt + Crd + Kfs resulting from contact metamorphism during the emplacement of ADA tonalite. In the lower Val Seniciaga, ADA tonalite includes Amp-rich layers and enclaves of RDC tonalite (Figure 4). ADA is a medium to coarse-grained tonalite exhibiting a massive texture. MOG crosscut all the aforementioned lithologies and consist of Qz-rich, fine to coarse-grained granitoids showing a fluidal texture, with rare Bt and lacking Hbl. No absolute ages are available for both MPD and MOD, even if intrusive relationships between MOD, MPD,

RDC and ADA tonalites suggest a chronologic order of emplacement in which gabbroic rocks (MPD) and diorites (MOD) are the oldest rocks. The amphibole compositions of MOD, MPD and MCD diorites change from Tschermakite to Mg-Hbl (Table S9, Figure S8). Barometric calculations on amphiboles of the RDC and ADA tonalites in the M. Ospedale area, wrapping diorite bodies, delivered pressure estimates between 3.5 and 5 kbar [76] (Tables S10 and S11).

4. Results

Based on whole-rock and isotopic compositions, a geochemical modelling allowed the detection the parental melt for Corno Alto–M. Ospedale rocks and the quantitative reconstruction of a differentiation path for such a melt, constraining magmatic petrogenesis. Afterwards, we tested potential contamination by modelling crustal anatexis to identify the type of the involved crustal melt.

4.1. Whole-Rock Geochemistry

Corno Alto-M. Ospedale rocks encompass a wide compositional range; a single lithotype (e.g., MOD) may show rather variable chemical compositions. A ternary diagram of normative albite (Ab) anorthite (An) orthoclase (Or) shows that all felsic rocks display more Ab-rich compositions (Figure 8). CATr samples occupy a borderline field between pure trondhjemite field ($An_{<30}$) and tonalite ($An_{>30}$); one CATr sample is classified as granite (sample A77-9). MPG (samples GZ181, GZ182) are set on the trondhjemite–granite border. CAT samples also place close to the tonalite–trondhjemite border but with an An wt.% slightly higher than CATr. SOS samples show a wide range of compositions from tonalite (samples A78-31 and A77-10) to granodiorite (AO4). These results are also corroborated by PCA statistical analysis of the Corno Alto felsic rocks showing how CAT and CATr plot into different clusters whereas SOS samples are more scattered, inferring more heterogeneous compositions (Figure S9).
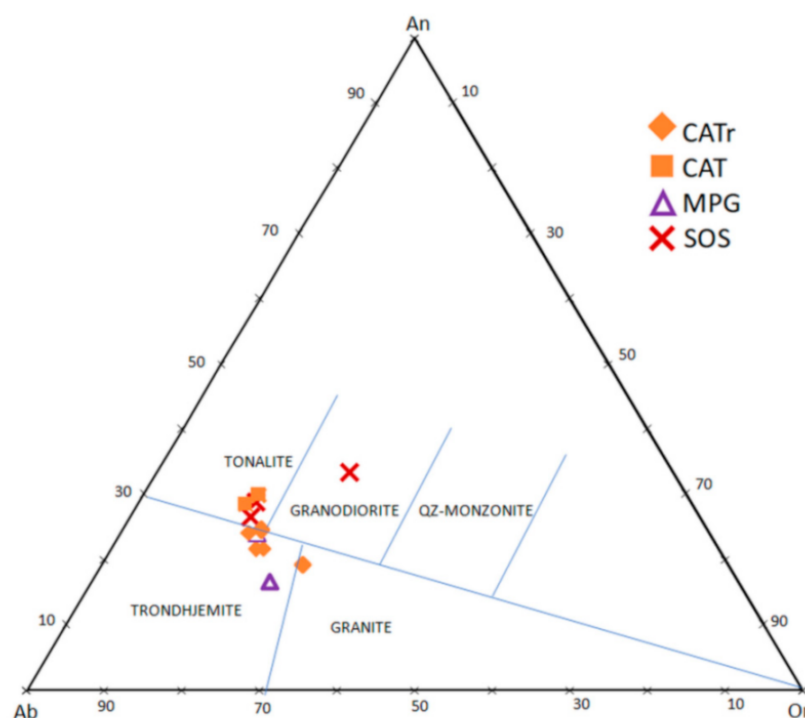

Figure 8. Ab–An–Or ternary diagrams for Corno Alto-M. Ospedale felsic samples. After Barker [77].

An efficient classification method for feldspathic igneous rocks is the MALI vs. SiO$_2$ diagram (Figure 9; Frost and Frost, 2008 [78]). All Corno Alto-M. Ospedale rocks plot in the lowest calcic field close to the calcic–calc-alkalic boundary (some samples fall onto the

boundary). Mafic samples plot left of the diorite field whilst CAT, CATr and SOS granitoids fall in the tonalite field or between tonalite and trondhjemite fields (as seen for Ab-An-Or diagram; Figure 8).
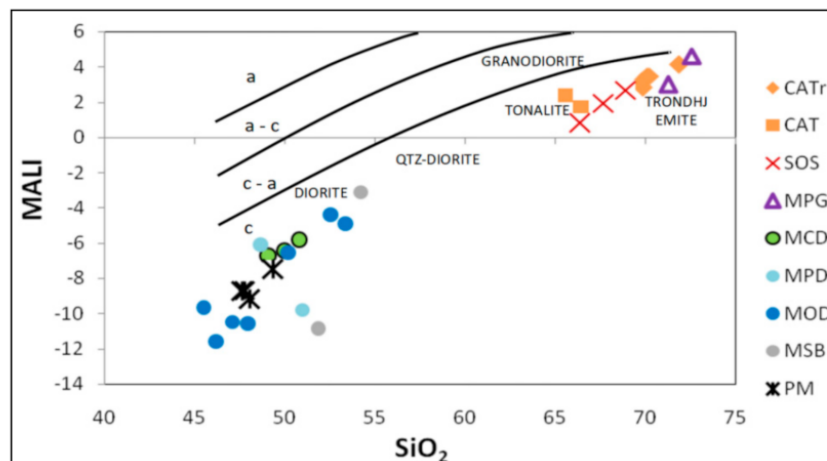

Figure 9. MALI classification diagram as a function of SiO_2 [78]. MALI stands for modified alkali–lime index ($Na_2O + K_2O$–CaO). CATr = Corno Alto trondhjemite, CAT = Corno Alto tonalite, SOS = Sostino granodiorite, MPG = Monte Palone granite, MCD = Malga Campo diorite, MPD = Malga Persec diorite, MOD = Monte Ospedale diorite, MSB = Malga Seniciaga Bassa diorite, PM = Parental melts. PM samples are Re di Castello Parental Melts after [16,23,25,31].

4.1.1. Major and Minor Elements

Major and minor elements compositions for both mafic and felsic samples (Table 2) are plotted against SiO_2 contents in the Harker diagrams (Figure 10). Supplementary Material reports the chemical and isotopic compositions and the Harker diagrams of the Re di Castello and M. Marser mafic rocks for comparison with Corno Alto-M. Ospedale samples (Tables S2–S4; Figure S10). The studied samples show a marked compositional heterogeneity, with SiO_2 ranging from 44 to 72 wt.%. The mafic samples cover a wide compositional span from 44.4 (sample VF164, MOD) to 53.6 (sample MK9, MOD) SiO_2 wt.%, whereas felsic rocks show a narrower interval of SiO2 values between 65.03 (sample GZ184, CAT) and 72.05 (GZ182, MPG) wt.%. A peculiar lack of intermediate terms is observed as no Corno Alto-M. Ospedale samples plot in the range between 55 and 65 SiO_2 wt.% (Daly Gap; [79]). RDC tonalite samples fill the Daly Gap shown by Corno Alto–M. Ospedale samples (Figure S10). Al_2O_3 contents are always >12 wt.%, excluding sample VF164. CAT and MCD display Al_2O_3 peaks with contents above 19%, while MOD exhibits rather variable Al_2O_3 contents. Al_2O_3 depicts a bell-shaped trend as it increases as SiO_2 decreases for diorites while an opposite tendency is displayed by felsic rocks (Figure 10). Ferromagnesian oxides (MgO, FeOtot) TiO_2, CaO and MnO have an overall negative correlation with SiO_2, whilst Na_2O and K_2O exhibit a positive correlation with SiO_2; P_2O_5 contents are roughly constant as SiO_2 increases, yet samples VF109, VF164 and MK9 (MOD) show high P_2O_5 contents ($P_2O_5 > 1$ wt.%, up to 2.09 for MK9).

4.1.2. Trace Elements

Elements such as Rb, Ba and Sr display similar trends with roughly increasing contents as SiO_2 increases (Tables 3 and S3). Despite their mafic composition, MCD exhibit high Sr contents (654 to 783 ppm), matching felsic rock. On the other hand, Rb and Ba contents for MCD are low (26 to 50 and 234 to 282 ppm, respectively), whereas some MOD and MSB samples appear to be enriched in these elements (up to 100 and 741 ppm). Mafic samples (VF109, VF164) show anomalously high compositions in Rb and Ba (VF164 has 135 ppm of Rb and 1934 ppm of Ba). These contents are even higher than felsic samples ones. Similar high La and Zr contents are displayed by the same samples. Excluding MCD

samples (lower Zr) both mafic and felsic samples fall in the same range of Zr contents (between 50 and 150 ppm). La contents display a slight positive correlation with SiO_2. Cr has higher contents for diorites (up to 641 ppm, sampleA3355). It decreases abruptly from PM samples (~600 ppm) to MCD (<30 ppm). PM samples are the parental melts suggested for Re di Castello pluton petrogenesis. Interestingly, MCD samples have similar Cr as felsic rocks, despite their lower SiO_2 (47–48 vs. 65–72 wt.%). One MSB sample has an extremely high Cr content of 1150 ppm. Primitive-mantle normalized patterns (Spider diagram) display an overall negative slope, due to an enrichment in less compatible elements: the concentrations of Rb, Ba, Th, U are >30 times those of primitive mantle. The enrichment factor decreases to <10 for HREEs (Figure S13).

Table 2. Major element compositions of Corno Alto–M. Ospedale samples and Re di Castello Parental Melts (PM) after [16,23,25,31]. Samples marked by * after Macera et al. [22].

| Sample	Rock	SiO_2	TiO_2	Al_2O_3	FeOt	MnO	MgO	CaO	Na_2O	K_2O	P_2O_5	LOI
A77-5 *	CATr	69.76	0.22	16.85	1.94	0.12	0.9	2.96	4.43	1.99	0.17	0.59
AP2	CATr	69.43	0.28	16.8	2.39	0.09	0.85	3.23	4.56	1.82	0.05	0.59
A2432	CATr	69.6	0.29	16.2	2.84	0.13	1.08	3.25	4.21	1.87	0.14	0.61
A77-9 *	CATr	71.54	0.25	15.5	1.98	0.12	0.78	2.56	3.99	2.69	0.13	0.39
A78-33 *	CATr	69.59	0.23	17.1	1.97	0.11	0.9	2.9	4.3	2.06	0.14	0.64
GZ183	CAT	65.84	0.39	18.02	3.16	0.08	1.26	4.25	4.31	1.65	0.19	0.76
GZ184	CAT	65.03	0.31	19.22	2.21	0.06	0.9	4.49	5.11	1.76	0.13	0.75
A78-31 *	SOS	67.02	0.51	16.57	3.08	0.07	1.28	4.2	4.42	1.71	0.24	0.73
A77-10 *	SOS	68.6	0.36	16.62	2.26	0.06	1.14	3.88	4.74	1.82	0.13	0.3
AO4 *	SOS	65.98	0.55	15.94	3.83	0.12	2	5.01	3.15	2.69	0.21	0.4
GZ182	MPG	72.05	0.18	15.92	1.53	0.08	0.51	2.18	4.37	2.39	0.09	0.64
GZ181	MPG	70.87	0.27	16.46	1.85	0.04	0.68	3.09	4.24	1.84	0.07	0.59
A2638	MCD	47.99	1.16	19.21	10.26	0.15	5.29	10.13	2.02	1.56	0.15	1.48
A2639	MCD	48.77	1.13	18.6	9.3	0.15	5.92	9.89	2.72	0.9	0.29	1.88
AP6	MCD	50.1	1.08	18.6	9.89	0.14	5.42	9.47	2.59	1.17	0.26	1.72
A3355	MPD	49.63	1.16	12.85	9.04	0.2	10.31	11.83	1.46	0.85	0.12	2.19
A3356	MPD	46.69	1.36	16.08	10.4	0.25	9.37	8.73	0.49	2.41	0.26	3.57
A3357	MOD	49.11	1.16	19.53	8.79	0.19	5.29	9.99	2.33	1.28	0.27	1.72
A3358	MOD	46.49	1.26	16.78	9.07	0.15	9.55	11.94	1	0.72	0.1	2.63
MK6	MOD	51.6	1.22	13.7	8.70	0.19	10.11	8.47	2.05	2.13	0.1	2.10
MK9	MOD	53.6	1.37	16.4	9.76	0.23	3.13	9.42	2.39	2.14	2.1	1.79
VF109	MOD	44.4	2.36	12.4	11.57	0.27	11.11	12.05	0.4	0.54	1.1	3.09
VF151	MOD	46.1	3.14	15.8	13.90	0.25	2.95	12.98	1.01	1.73	0.11	2.58
VF164	MOD	44.4	1.91	9.6	12.94	0.28	13.68	11.59	0.31	1.86	1.1	2.7
MK4	MSB	52.8	1.27	17.1	7.41	0.13	5.87	7.87	3.86	1	0.14	3.08
VF102	MSB	51.0	1.87	13.3	10.46	0.18	6.50	12.83	0.88	1.3	0.09	2.1
JM158c	PM	46.0	0.7	12.42	9.14	0.18	16.53	10.02	1.18	0.39		2.6
C1	PM	47.54	0.73	13.31	9.42	0.17	16.43	10.33	1.25	0.45		
JM157	PM	46.93	0.79	13.83	7.98	0.14	12.64	9.89	2.24	0.51	0.16	4.11
U237	PM	46.29	0.77	15.45	8.21	0.16	11.5	11.32	1.66	0.8	0.15	3.69
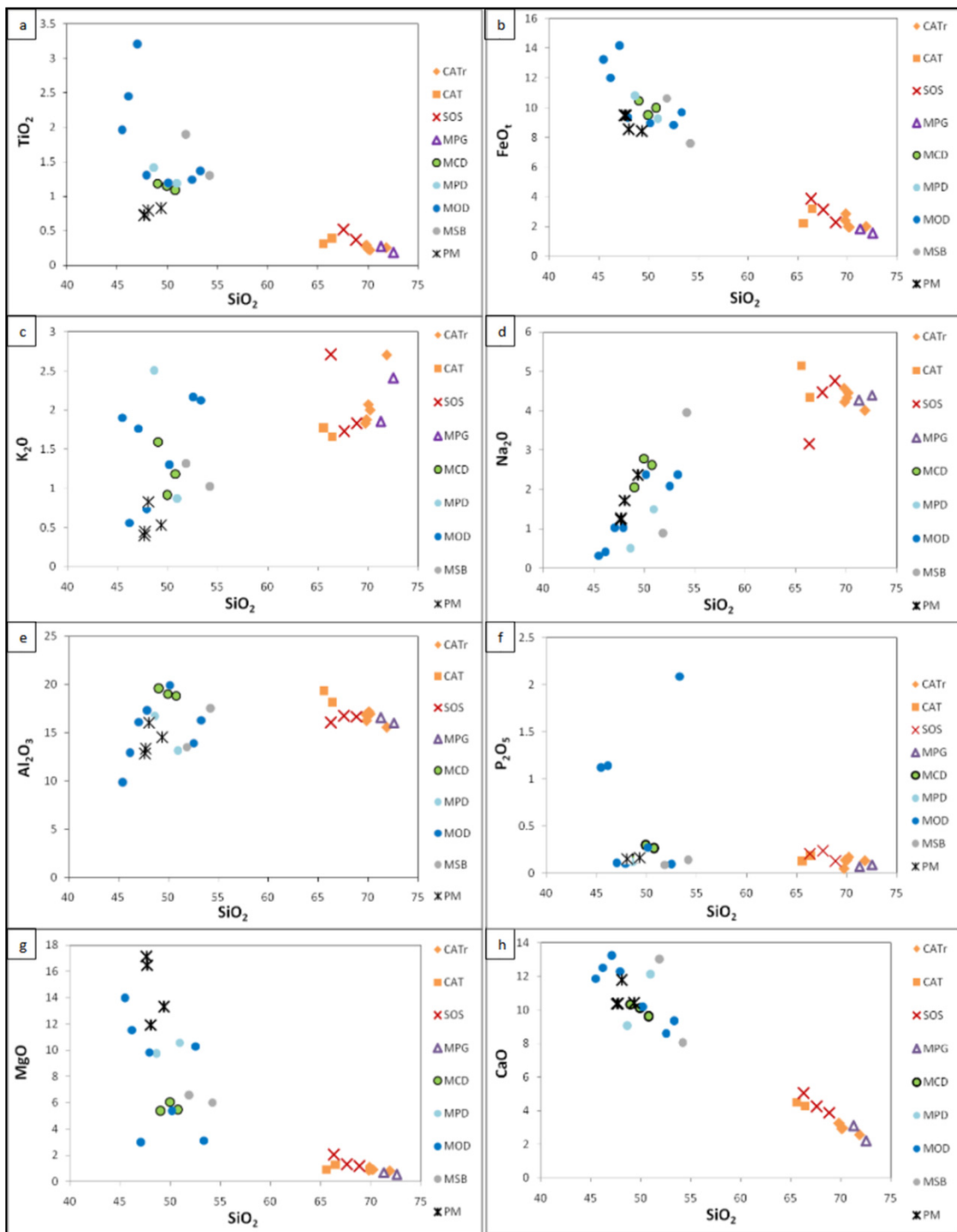
Figure 10. *Cont.*
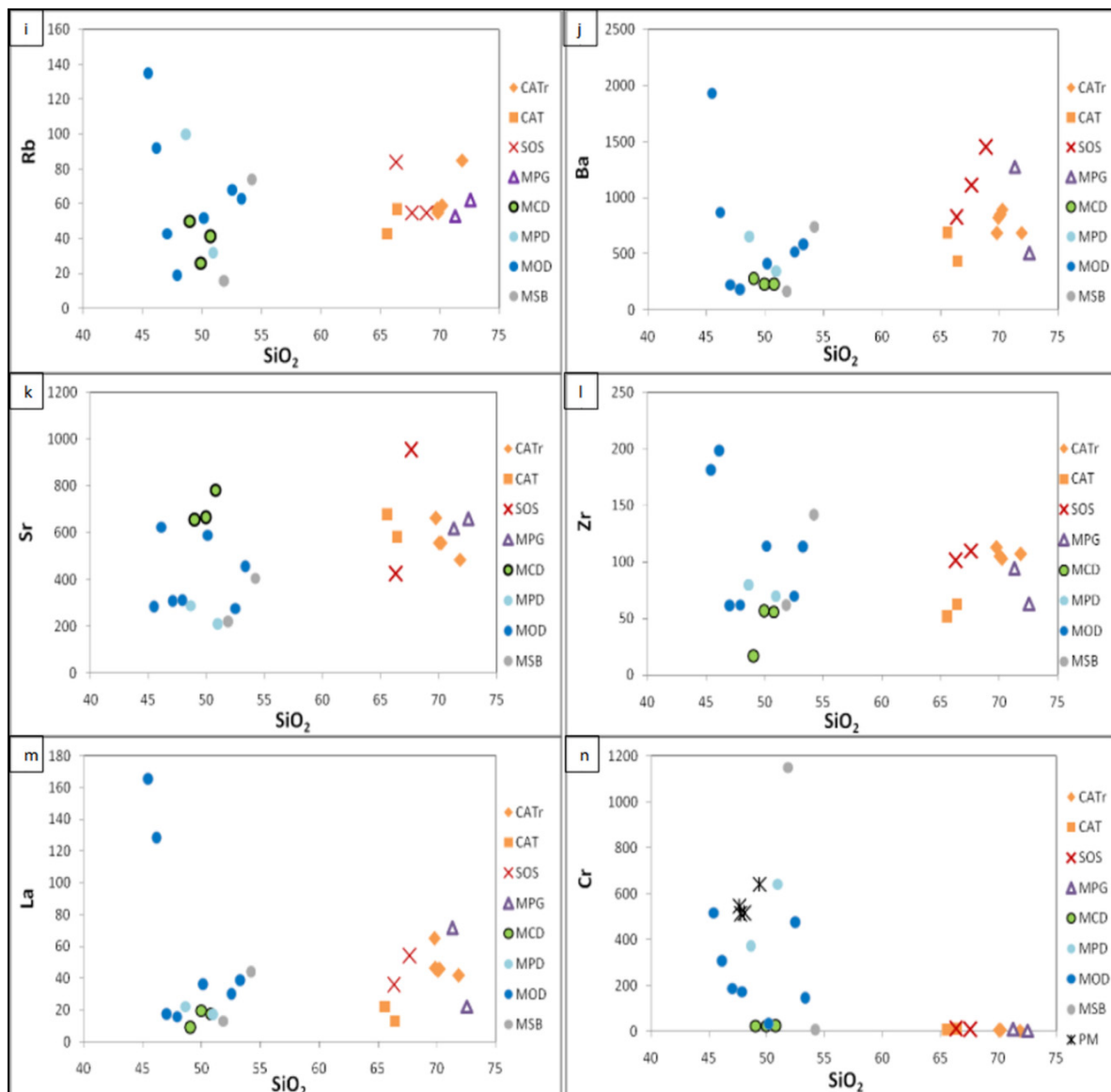
Figure 10. Harker diagrams for Corno Alto–M. Ospedale samples. (**a–h**) Major elements (**i–n**) Trace elements and REE. Symbols as in Figure 8.

4.1.3. Isotope Geochemistry

In the plot SiO$_2$ versus ^{87}Sr/^{86}Sr (Figure 11a), a first recognizable feature is the isotopic similarity between MCD and the mafic parental magmas from the literature (^{87}Sr/^{86}Sr < 0.705) (Tables 4 and S4). Such Sr isotopic compositions underline a lithospheric mantle affinity for MCD [61]. In contrast, the other mafic lithologies from Corno Alto, which include MOD (except for two samples), MSB and MDP, have more radiogenic values than MCD that are similar to the most differentiated units (SOS, CAT and CATr) within the interval between 0.7054 and 0.7082. A little amount of crustal contamination (assuming a crust with ^{87}Sr/^{86}Sr > 0.735) may have affected the trondhjemites, granites and granodiorites, according to Del Moro et al. [8]. The diagram Sr isotopic ratio vs. εNd (Figure 11b) shows that among the considered rock suites, only the Southern Re di Castello gabbro reveal mantle affinity with εNd > 0 and low ^{87}Sr/^{86}Sr (Figure S11b). Additionally, MPD and MCD show εNd ≈ 0 or slightly negative and low to medium ^{87}Sr/^{86}Sr values thus displaying little amounts of crustal assimilation. CATr, CAT, SOS and MOD lie in the εNd < 0—high ^{87}Sr/^{86}Sr sector, emphasizing crustal assimilation (Figure 11b).

Table 3. Trace elements and rare earth element (REE) compositions of Corno Alto–M. Ospedale samplesand Re di Castello Parental Melts (PM) after [16,23,25,31]. Samples marked by * after Macera et al. [22].

Sample	Rock	Cs	Rb	Ba	Th	U	Nb	Ta	La	Ce	Pb	Pr	Sr	Nd	Zr	Hf
A77-5 *	CATr	1.5	59	898	15.3	2.6	18.5	1.59	45.6	76.5	27.6	6.64	556	22.4	103	2.78
AP2	CATr		57	688	27.5	2.5	18		65.1	108		10.27	663	36.3	113	
A2432	CATr		55	823					46.1	74.4		7.17		23.4		
A77-9 *	CATr	3.8	85	690	15.9	2	16.7	2.01	41.9	70.6	32.8	6.55	485	22	107	3.03
A78-33 *	CATr	1.5	57.8	851	15.4	2.5	18.2	1.48	44.7	75.7	27.6	6.64	556	22.4	105	2.77
GZ183	CAT		57	439			8		13.1	25.2			583		63	
GZ184	CAT		43	693			4		22.2	30.2			680		52	
A78-31 *	SOS		55	1116	17.8	5.67	22		54.3	90.8		8.71	954	27.7	110	
A77-10 *	SOS		55	1452	22.7	7										
AO4 *	SOS		84	824	21.2	6.6	17		36.1	58		5.95	424	21.2	101	
GZ182	MPG		62	505			11.1		22.2	46.4			659		63	
GZ181	MPG		53	1278			28		71.6	121		11.51	619	35.8	94	
A2638	MCD		50	282	3.1	2.8	6		9.2	23.6		3.61	654	16.3	17	
A2639	MCD		26	234	4.4	5.9	8		19.7	42		5.31	664	22	57	
AP6	MCD		41	235	6.6	4.5	6		17.5	38.3		4.75	783	20.2	56	
A3355	MPD		32	348	5.3	1.9	8		17.2	31.5		3.62	212	15.2	70	
A3356	MPD		100	656	6.4	3	15		22.2	47.9		5.89	289	24.7	80	
A3357	MOD		52	411	11.8	3.4	11		35.9	72		8.01	590	32	114	
A3358	MOD		19	180	4.8	1.7	5		15.8	35.8		4.56	310	20.1	62	
MK6	MOD	2.4	68	519	8.7	3.2	11.7	1.08	29.9	65.5	7.6	7.39	277	29.6	70	2.33
MK9	MOD	2	63	583	10.1	3.6	16.5	1.18	38.5	79.7	9.1	9.26	455	37.9	113	2.9
VF109	MOD	3.2	92	871	33.1	6.5	48.2	3.01	128	228	8	24.1	624	86.2	198	4.47
VF151	MOD	1.7	43	226	3.8	0.8	8	0.54	17.2	35.2	4.7	4.42	306	19.9	61	2.23
VF164	MOD		135	1934	48.5	12.1	33		165	268		27.16	282	96.6	181	
MK4	MSB	1.2	74	741	14.2	2.4	14.3	1.18	44.2	78.3	26.7	7.79	406	27.7	142	3.55
VF102	MSB	0.2	16	167	3.2	0.7	7.4	0.55	13.1	28.3	3.72	3.58	222	15.7	62	1.93
JM158c	PM															
C1	PM															
JM157	PM		12	172								5		272		64
U237	PM		12	92	5	1	3					6		416		43
Sample	Rock	Sm	Eu	Gd	Tb	Dy	Y	Ho	Er	Tm	Yb	Lu	Ni	Co	Cr
A77-5 *	CATr	3.14	0.9	2.08	0.33	1.81	11.3	0.38	0.97	0.17	1.08	0.18	4	2	4.7
AP2	CATr	6.05	1.36	4.84	0.62	2.77	15	0.57	1.3	1.19	1.36	0.2			
A2432	CATr	3.45	1.01	2.84	0.38	2.14		0.43	1.19	0.19	1.32	0.22			
A77-9 *	CATr	3.47	0.9	2.57	0.4	2.33	13.8	0.47	1.21	0.21	1.37	0.22	3.2	2.3	3.7
A78-33 *	CATr	2.99	0.9	2.26	0.34	1.73	11.6	0.37	0.96	0.16	1.1	0.18	4.2	2.1	6
GZ183	CAT						10						6	8	13
GZ184	CAT						6						4	5	9
A78-31 *	SOS	3.78	1.17	3.62	0.58	3.07	18	0.73	1.71	0.26	1.76	0.25	83	41	641

<div align="center">Table 3. Cont.</div>

Sample	Rock	Sm	Eu	Gd	Tb	Dy	Y	Ho	Er	Tm	Yb	Lu	Ni	Co	Cr
A77-10 *	SOS														
AO4 *	SOS	3.81	1.06	3.23	0.42	2.62	16	0.59	1.54	0.25	1.65	0.23	8		11
GZ182	MPG	4.98	1.32	3.71	0.44	2.13	13	0.39	1.01	0.15	1.06	0.18	2	2	4
GZ181	MPG						16						4	3	8
A2638	MCD	4.45	1.25	3.94	0.62	3.79	21	0.83	2.02	0.3	1.9	0.28	9	41	24
A2639	MCD	5.17	1.48	4.29	0.68	3.78	22	0.84	2.08	0.32	1.95	0.28	19	36	24
AP6	MCD	4.59	1.32	3.96	0.61	3.57	19	0.79	1.89	0.28	1.9	0.28	20	35	27
A3355	MPD	3.78	1.17	3.62	0.58	3.07	18	0.73	1.71	0.26	1.76	0.25	83	41	641
A3356	MPD	5.71	1.76	4.56	0.71	3.99	23	0.88	2.13	0.33	1.97	0.3	72	46	373
A3357	MOD	5.87	1.72	5.17	0.78	4.17	23	0.93	2.34	0.35	2.26	0.35	16	31	32
A3358	MOD	4.55	1.32	4.31	0.68	3.95	21	0.89	2.05	0.31	1.93	0.28	185	47	174
MK6	MOD	5.48	1.47	4.7	0.72	3.98	25	0.93	2.29	0.36	2.35	0.39	147	35	473
MK9	MOD	7.19	1.73	5.69	0.84	4.61	27	0.99	2.46	0.38	2.62	0.43	46	27	143
VF109	MOD	13.38	3.6	9.47	1.23	5.79	25	1	2.26	0.27	1.59	0.22	264	46	306
VF151	MOD	5	1.49	5.04	0.71	4.19	22	0.91	2.05	0.34	1.89	0.26	43	36	188
VF164	MOD	14.54	3.44	11.3	1.19	5.47	23	0.94	2.05	0.23	1.59	0.23	341	57	517
MK4	MSB	4.6	1.13	3.45	0.53	2.79	18	0.61	1.6	0.24	1.75	0.29	7	4	9
VF102	MSB	3.83	1.18	3.88	0.55	3.34	19	0.76	1.73	0.28	1.67	0.24	122	37	1150
JM158c	PM														547
C1	PM														513
JM157	PM						17							217	642
U237	PM						8							154	36	518

Table 4. Sr–Nd data for Corno Alto-M. Ospedale samples. Sr initial ratios and εNd have been calculated at t = 40 Ma. Isotopic data of samples marked by * after Del Moro et al. [8].

Sample	Rock	Rb (ppm)	Sr (ppm)	$^{87}Rb/^{86}Sr$	$(^{87}Sr/^{86}Sr)_i$	Error	$(^{87}Sr/^{86}Sr)_t$
AP2	CATr	57	663	0.2480	0.706176	0.000009	0.706035
A77-9 *	CATr	85	485	0.5072	0.706775	0.000011	0.706487
A78-33 *	CATr	58	556	0.3019	0.706004	0.000016	0.705832
A78-31 *	SOS	55	954	0.1675	0.706381	0.000013	0.706286
A2638	MCD	50	654	0.2214	0.704625	0.000009	0.704499
A2639	MCD	26	664	0.4217	0.704607	0.000013	0.734666
AP6	MCD	41	783	0.1515	0.704671	0.000018	0.704578
MK6	MOD	68	277	0.7149	0.707328	0.000022	0.706924
MK9	MOD	63	455	0.4014	0.707072	0.000012	0.706844
VF109	MOD	92	624	0.4289	0.709337	0.000014	0.709095
VF151	MOD	43	306	0.4175	0.706909	0.000011	0.706678
VF164	MOD	135	282	1.3855	0.710311	0.000016	0.706139
MK4	MSB	74	406	0.5794	0.708625	0.000010	0.708318
VF102	MSB	16	222	0.2292	0.706257	0.000018	0.706133

Table 4. *Cont.*

Sample	Rock	Sm (ppm)	Nd (ppm)	$^{147}Sm/^{144}Nd$	$^{143}Nd/^{144}Nd$	Error	εNd_t
A77-5 *	CATr	3.14	22.40	0.08480	0.512492	0.000015	−2.28
AP2	CATr	6.05	36.30	0.10080	0.51247	0.00001	−2.71
A77-9 *	CATr	3.47	22.00	0.09538	0.512416	0.000011	−3.81
A78-33 *	CATr	2.99	22.40	0.08070	0.512502	0.000006	−2.06
A7831 *	SOS	3.78	27.70	0.08250	0.512432	0.000009	−3.44
A2638	MCD	4.45	16.30	0.16510	0.512485	0.000027	−298
A2639	MCD	5.17	22.00	0.14210	0.512551	0.000034	−1.42
AP6	MCD	4.59	20.20	0.13740	0.512509	0.000012	−2.21
MK6	MOD	5.48	29.60	0.11200	0.512361	0.000024	−4.97
MK9	MOD	7.19	37.90	0.11470	0.512410	0.000015	−4.03
VF109	MOD	13.38	86.20	0.09390	0.512543	0.000006	−1.33
VF151	MOD	5.00	19.90	0.15190	0.51246	0.000011	−3.47
VF164	MOD	14.54	96.60	0.09100	0.512507	0.000005	−2.56
MK4	MSB	4.60	27.70	0.10042	0.512321	0.000008	−6.18
VF102	MSB	3.83	15.70	0.14750	0.512581	0.000008	−1.1
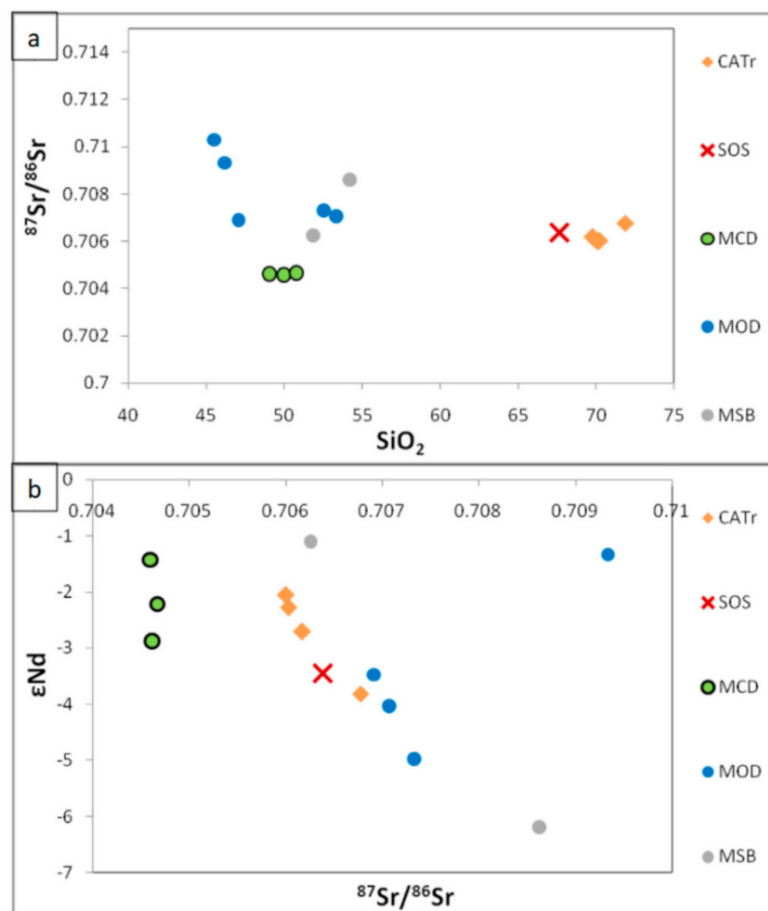
Figure 11. (**a**) SiO_2 vs. $^{87}Sr/^{86}Sr$ diagram for Corno Alto–M. Ospedale rocks. (**b**) $^{87}Sr/^{86}Sr$ vs. εNd diagram for Corno Alto–M. Ospedale samples. Symbols as in Figure 8.

4.2. Modelling

As pointed by the geochemistry, the Corno Alto pluton shows a wide range of compositions, thus, to understand the possible process that contributed to such variation we conducted a geochemical modelling of fractional crystallization of possible parental mafic magmas and partial melting of crustal lithologies. The results can be found in Figure 12 and Tables S5–S8.

In the first approach, we evaluated the effect of fractional crystallization and evolution of an initial mafic magma. The model was run using the software Rhyolite-Melts v 1.2.0 (details in Section 2) and all starting compositions were at Quartz–Fayalite–Magnetite (QFM) buffer, constant pressure of 4 kbar, and contained 4 wt.% H_2O. The crystallization was then evaluated at increments of 50 °C until complete cooling. The solid assemblages and the evolution of fractionated melt compositions at each step are presented in Figure 12a,b, respectively.

The four selected parental magmas start the crystallization of Ol at temperatures between 1190 and 1260 °C. Ol is the only phase present until 10–13% solidification, and is followed by the crystallization of Sp and Cpx between 10 and 50% solidification. Opx appears at different steps depending on the sample, as early as at 46% in MK6 and 54% in A3355, and later than >65% in JM157 and U237 (Figure 12a). Hydrous phases such as Hbl and Bt crystallize only after >65% crystallization. In particular, for sample JM157, Hbl is a significant phase reaching proportions between 28 and 32 modal%. Similarly, in U237, the amount of Hbl in the final steps of crystallization may reach 17 modal%. In contrast, MK6 contains only a few percent Hbl (2.5 modal%), and A3355 does not crystallize amphibole. Pl appears as early as at 65% of crystallization (MK6), but usually at >84% solidification. Simulations ended at temperatures between 820–850 °C.

In Figure 12b the evolution of the parental magmas usually started at <50 wt.% SiO_2 and the fractional crystallization produced melt compositions with SiO_2 between 61.3 to 68.6 wt.% which are generally below the most fractionated rocks from Corno Alto (MPG, CAT, SOS and, especially, CATr) that reach up to 72 wt.% SiO_2. Models for JM157 and U237 produced the less evolved end members, conversely model MK6 and A3355 reached slightly higher SiO_2 contents. In the case of MgO, FeOtot and Na_2O the general trends overlap some of the natural samples from SOS and CAT, in particular, model MK6 seems to the best representative. On the other hand, the CaO trend is only partially reproduced by the models, because although the melts evolve in the right direction and overlap with SOS and CAT, the lowest values, for unit CATr, are not reproduced. The poorest correlation of the models is observed for K_2O as they completely fail to reproduce its behavior, since the evolved compositions have much higher contents (>3 wt.%) than the natural samples.

As described above, a simple fractional crystallization of a mafic parental magma fails to reproduce the most differentiated rocks from Corno Alto. This suggests that other processes may be involved in their formation. To investigate the possible involvement of crustal melts in the genesis of Corno Alto pluton, we modeled crustal anatexis. Both African and European lower and upper crust sections, involved in the Europe–Adria collision, were considered as possible crustal sources (Table 5). A possible contribution to Adamello rock genesis from the European lower Continental Crust (ELC) was first advised by von Blanckenburg and Davies [80]. European lower crust samples from Massif Central [81], Pannonian Basin [82], Eifel Volcanics [83], Calabria Serre Basement [36] and Adriatic lower crust rocks from the Ivrea Body [38] have all been taken into consideration for thermodynamic modelling. Moreover, the Southalpine upper crust is represented in the Adamello area by the Edolo Schists and Massiccio delle Tre Valli Bresciane phyllites (TVB) [24,37,64] has also been taken into account. Four samples were selected for Perple_X processing [34] according to a paleogeographic criterium: in particular, at the time of Corno Alto intrusion (43 Ma), the Serre basement has been considered as a portion of the Sardinia–Corse promontory of European affinity [84–87]. The selected samples are described below.
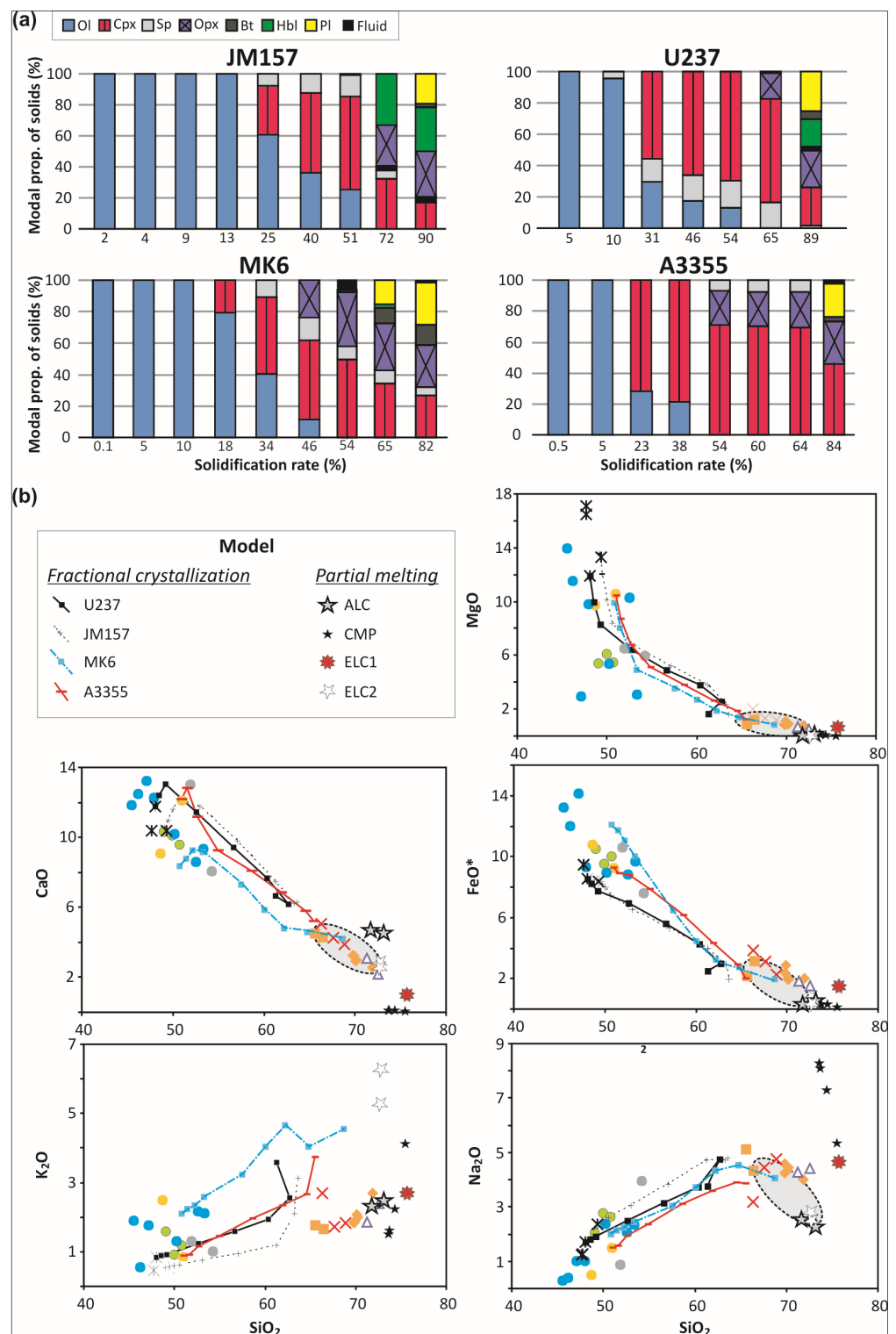
Figure 12. (**a**) Results of fractional crystallization of four possible parental magmas: JM157 [31], U237 [16], MK6 (MOD) and A3355 (MPD). Bar diagrams represent modal proportion of solids at each step of crystallization (mineral abbreviations after Whitney and Evans [30]). (**b**) Harker diagrams of the rocks from the Corno Alto (symbols as in Figure 8) and the obtained model melt compositions from fractional crystallization (JM157, U237, MK6 AND A3355) and partial melting (ALC, CMP, ELC1 and ELC2) simulations.The grey fields represent rocks composition formed by the combination of partial melting and fractional crystallization processes. Note that FeO* represents all iron as Fe^{2+}.

Table 5. Major elements composition and equilibrium P-T conditions of Perple_X protoliths.

Sample	ELC1	ELC2	ALC4	CMP
T (°C)	760–800	830	850–900	400–425
P (kbar)	6.5–7	8	8.3–9	34
SiO_2	50.01	48.61	48.08	59.48
TiO_2	1.78	1.32	0.32	0.89
Al_2O_3	18.98	17.55	26.23	20.71
FeOt	14.05	9.34	5.69	6.52
MnO	0.3	0.19	0.2	0.07
MgO	6.56	7.26	4.32	1.86
CaO	4.17	10.23	12.17	0.1
Na_2O	1.42	2.89	2.1	1.43
K_2O	0.52	0.68	0.2	4.08
H_2O	1.84	1.25	0.06	4.52

ELC1 is a Grt-Crd-bearing granulite from the Serre basement, Calabria, South Italy, displaying metamorphic peak P-T estimates of 760–810 °C and 6.5–7 kbar (LCCC, [36,88]).

ELC2 is a layered granulite-facies metagabbro from the Serre basement, Calabria yielding P-T peak conditions of 780–820 °C and 7–8 kbar (LCCC, [36,88]).

ALC4 is an Ivrea metagabbro, Northern Italy whose calculated metamorphic peak condition is 800–850 °C and 8.3 kbar [38,89].

CMPis a white mica-bearing phyllites with high Qz contents, from the Central Southalpine basement of the "Massiccio delle Tre Valli Bresciane (TVB)" [37]. Final equilibrium at intermediate crust P-T conditions have been suggested for this basement [64].

For each composition, a P-T pseudosection has been calculated (Figure S12). The compositions of anatectic melts produced at variable P-T conditions are reported in Table 6. Nine major element compositions of melts were calculated, at different P-T conditions, according to available geothermobarometric data. The melt amounts range from 5 to 12 vol.% for different P-T conditions (Table 6). These degrees of partial melting are consistent with the degree of crustal assimilation suggested by geochemical constraints [8]. In these calculations, we assume that crustal melts were produced at deeper levels (6.5 to 10 kbar) with respect to the emplacement depths suggested for the Corno Alto granitoids.

The melt composition calculated from ELC1 sample (Serre metapelite) is a silica-rich melt, poor in ferromagnesian oxides but rich in Na_2O and Al_2O_3. Two melts were calculated from ELC2 sample (Serre section metagabbro). Both melts are silica-rich and show the highest contents of K_2O among calculated melts, moderate CaO, low Na_2O and negligible amounts of FeOtot and MgO (Table 6). Two melts were obtained from ALC4 melting (Ivrea metagabbro). They were computed at the same T (900 °C), but at different pressures (8 and 10 kbar). Computed ALC4 melt compositions partially resemble those obtained from the melting of ELC2 metagabbro even if the former display higher Al_2O_3, CaO contents while a conspicuous K_2O reduction is predicted in ALC4 melts (Table 6). K_2O content of ALC4 melts are less than the half of ELC2 ones. Four melts were computed considering the average composition of the phyllites from Massiccio Tre Valli Bresciane (TVB) as protolith. The P-T conditions selected for melt production are typical of intermediate–upper crustal levels. These melts are characterized by the lowest CaO contents and the highest Na_2O values and show the largest variations in terms of K_2O and Na_2O concentrations.

Table 6. P-T conditions, partial melting degrees and major elements compositions for Perple_X computed melts.

Sample	ELC1	ELC2	ELC2	ALC4	ALC4	CMP	CMP	CMP	CMP
T (°C)	760	800	850	900	900	675	680	675	665
P (kbar)	6.5	8	8	8	10	10	10	8	5
Vol % melt	6	5	9	5	8	5	11	9	12
SiO_2	67.68	68.62	69.15	69.24	67.3	62.97	63.19	64.81	68.08
Al_2O_3	12.36	14.56	14.64	16.03	17.16	13.71	13.69	13.64	13.39
FeOt	1.3	0.36	0.76	0.51	0.3	0.32	0.31	0.28	0.11
MgO	0.57	0.08	0.14	0.16	0.08	0.1	0.1	0.07	0.02
CaO	0.91	2.43	2.76	4.28	4.39	0.07	0.08	0.08	0.04
Na_2O	4.17	2.37	2.67	2.13	2.39	7.09	6.95	6.34	4.83
K_2O	2.41	5.91	5.02	2.34	2.17	1.28	1.38	1.95	3.71
H_2O	10.6	5.68	4.85	5.32	6.22	14.46	14.3	12.84	9.81

5. Discussion

5.1. Petrogenesis of the Corno Alto Pluton

Harker diagrams display a typical trend of calc-alkaline series (Figure 11) [61]: MgO, FeOtot, CaO, TiO_2 and MnO decrease as SiO_2 increases owing to the early crystallization of mafic minerals. For instance, MgO and TiO_2 decrease exponentially due the crystallization of early phases such as Mg-Hbl, while alkali oxides (Na_2O and K_2O) increase as result of the preferential segregation of alkali-rich phases, as SiO_2 increases. High SiO_2 contents (>72 wt.%) are displayed by MPG, since M. Palone and M. Cornaccio are felsic differentiations of the main Corno Alto trondhjemitic body. On the other hand, SOS and CAT are slightly less evolved compared to the main CATr (65–68 vs. 69–71 SiO_2 wt.%), also displaying higher average compositions for CaO, MgO and FeOtot (up to 5.01, 2 and 3.83 wt.%, respectively). These samples could represent a medium-to-late crystallization stage with segregation of Bt, Ms and andesine Pl. Comparing SOS with CATr, the former shows values SiO_2, MgO, FeOtot, CaO and alkali values ranging from granodiorite (sample AO4) to trondhjemite (sample A77-10). Al_2O_3 values show a bell-shaped trend with the mafic flank of the curve being steeper than the felsic one. This is due to the higher modal abundances of Al-rich phases segregating at intermediate silica content. Samples showing P_2O_5 peaks also have high La contents, owing to higher modal proportions of Ap.

The trace element compositions of Corno Alto samples do not show a clear enrichment in incompatible elements in the most differentiate rocks. For instance, Ba is generally higher in felsic lithotypes; felsic and some mafic rocks (MCD and MOD) show similar Sr contents, ranging between 400 and 800 ppm. Some MOD, MPD and MSB samples have rather high Rb contents (Table 3), comparable with Corno Alto rocks ones (from 50 to 100 ppm). A similar scenario is depicted for Zr. Cr is the only compatible trace analyzed: it describes an exponential curve alike Mg and Ti owing to the early crystallization of Cr-rich phases. Sample VF102 (MSB), having an extremely high Cr content of 1150 ppm, could be considered as either a likely parental melt or a cumulate. Two MOD samples (VF109 and VF164) exhibit exceptionally high contents of all incompatible traces and REEs (Table 3). These samples are very fine-grained rocks, showing no phenocrysts.Thus, they have been interpreted as late magmatic mafic dykes retaining high concentrations of incompatible elements. MCD are mildly rich in Sr and Ba (mobile trace elements) whereas MOD, MPD and sample MK4 (MSB) display high contents for Ba, Rb, Zr and La (both mobile and immobile traces). To produce an enrichment in immobile traces, we must assume circulation of both melts and fluids in the same system [61]. Hence, metasomatism

by means of slab-deriving melts and fluids affected the mantle source that generated the parental melts [16,90]).

Primitive mantle-normalized trace and REE patterns confirm what stated above (Figure S13). MOD, MPD and MSB samples are mildly to highly enriched in Ba, Rb, Sr, U, Th and La (mobile and immobile traces) with enrichment factors up to 100. On the other hand, MCD samples show a clear enrichment in mobile traces such as U (enrichment factor > 150) and Sr (mobile traces). An evident Nb trough characterize the patterns of all rocktypes suggesting a crustal contribution to their petrogenesis. The latter can be ascribed to both subduction-related metasomatism and assimilation of crustal material.

Southern Re di Castello and M. Marser rocks have been taken into consideration for comparison purposes. It is worth noting how the absence of the Daly Gap for Southern Re di Castello rocks may suggest the occurrence of other magmatic processes or a contribution from sources different than the ones involved in the Corno Alto-M. Ospedale petrogenesis (Figure S10). Furthermore, M. Ospedale and M. Marser mafic rocks both exhibit high Al_2O_3 and FeOtot and $^{87}Sr/^{86}Sr$ maybe suggesting similar sources and/or petrogenetic processes (Table S2, Figure S11).

Samples A3355 (MPD) and MK6 (MOD) have been selected for fractional crystallization modelling due to their geochemical features: among MPD and MOD samples, A3355 and MK6 display the highest Cr (641 and 473 ppm), high MgO (10.31 and 10.11 wt.%) and relatively low $^{87}Sr/^{86}Sr$ values (0.70656 and 0.70683). These features partially match the ones suggested by Ulmer et al. for the Southern Re di Castello parental melt (PM sample U237, Tables 2 and 3, [16]).

Perple_X computed melt compositions are in agreement with hydrate minerals breakdown reactions, for the P-T conditions fixed for the modeling of each melt [91–94].

Despite thermodynamic modelling may suffer from some pitfalls [95], the obtained constraints may help to shed light on the genesis of this pluton. As described in the previous section, although there are compositional similarities among felsic CornoAlto–M. Ospedale rocks and computed melts obtained by fractional crystallization and partial melting, these processes do not seem to be mutually exclusive. Instead, the results presented here show that they may have played a role together. The most evolved samples of Corno Alto usually have compositions that are intermediate between melts produced by crustal anatexis and the melts produced after fractional crystallization (Figure 12b). This feature suggests that SOS, CAT and CATr could have been produced by the interaction of crustal and mantle derived magmas. Such idea is also reinforced by the lack of intermediate components between the mafic and felsic end-members (SiO_2 between 55–65 wt.%). In particular, melts from ELC1 (Serre metapelite) seems to represent the most probable felsic end-members that have played a role in the genesis of these rocks. A possible inconsistence of the fractional crystallization model consists of the prediction of a considerable crystallization of Ol, Cpx and Opx, which have not been observed in the mafic rocks from Corno Alto; instead, the most common mafic mineral is Hbl. It is possible that Ol-websterite cumulates are present in the unexposed roots of this pluton, as documented by the Ol + Sp clots of M. Mattoni (Southern Re di Castello) [90].

5.2. Geodynamic Setting during the Late Cretaceous-Eocene

The interpretation of the Adamello magmatism and, in particular, the emplacement of the earlier southern and eastern plutons of Re di Castello and Corno Alto during Eocene time in the Alpine scenario, needs a brief revision of the geodynamic models proposed for the evolution of the Eastern and Southern Alps.

During Early Cretaceous times, a south dipping slab was plunging beneath the eastern Southern Alps as indicated by the climax of Eo-Alpine high-pressure metamorphism in the Eastern Alps at about 90–100 Ma [96]; this is consistent with the onset of intra-Austroalpine SE-dipping subduction and collision [97,98]. Extrusion processes of high-P rocks taking places during 90–85 Ma, relate to rapid exhumation and erosion of the high-P Austroalpine units [98,99].

Oceanic subduction of the Alpine Tethys started probably in the Turonian, as testified by the accretion of ophiolitic material at the northern edge of the Adriatic microplate at about 90 Ma [100]. Eclogites embedded in the tectonic units of the Tauern Window give evidence of subduction metamorphism during Late Cretaceous–Eocene times [101–103].

The south-directed subduction of the Alpine Tethys to a depth of 70–80 km was followed by the collision between the Adriatic microplate and the European plate during Eocene, resulting in the formation of an orogenic wedge in which the Adria-derived Austroalpine units and the Europe-derived Penninic units were transported northwards [104–107]. Indications for S-directed subduction are provided by high-P metamorphism in the Tauern Window and in the Lower Austroalpine at 45–37 Ma [108,109]. This event is contemporaneous with high-P metamorphism in the Bunderschiefer of the Engandine Window, attributed to the subduction of the Valais oceanic crust and European sediments at 43–40 Ma, followed by rapid decompression/exhumation during the Late Eocene/Oligocene (36–33 Ma) [110,111]. Following this S-directed subduction, during Miocene the southern alpine crust east of the Giudicarie Fault System, started to indent the Eastern Alps, resulting in a 65 km N–S shortening north of the Periadriatic Lineament [112]. This changed fundamentally the configuration of the mantle slab beneath the Eastern Alps, with the formation of a NE-dipping Adriatic slab [113].

5.3. Late Cretaceous–Middle Eocene Tectonics in the Southern Alps

Quiescence/extensional tectonics which facilitated the Corno Alto intrusion is difficult to reconcile with the tectonic setting of the central Southern Alps during Late Cretaceous–Middle Eocene time [2,114,115]. West of Adamello, contractional structures involving the basement and the sedimentary cover were active during Campanian–Maastrichtian (80–68 Ma) and were reactivated during Paleocene–Middle Eocene times (56–43 Ma; [116]). These structures, linked to the ongoing Alpine subduction and collision active northward are sealed eastwards by the oldest plutons of the Adamello batholith [1,106,117–119]. Contractional tectonics is recorded in the Southalpine foredeep by 2000 m-thick terrigenous turbidites of Cenomanian to Campanian age, testifying the erosion of metamorphic rocks exposed in both Southalpine and Austroalpine units [115,120–122]. Turbidites were followed by hemipelagic sedimentation up to the Early/Middle Eocene, related to a waning stage of the contractional deformation [123,124]. Cretaceous to Middle Eocene thrusts are subsequently cut by normal faults intruded by andesitic dykes during the final stages of their activity at 42–39 Ma [11]. Faults are oriented E–W, WSW–ENE and NE–SW, partly reactivating former thrust contacts and displaying a maximum throw of about 200 m [11].

The Adamello batholith is bordered to the east by the South Giudicarie Fault zone (Figures 2 and 13), which shows extensional/transtensional activity along N- and NE-trending faults during the Late Cretaceous (Figure 13a) [52,53]. The same faults represented the eastern boundary for the deposition of the Late Cretaceous flysch, which was channeled along a NE-trending through allowing the transport of coarse-grained clastic deposits sourced from the Austroalpine nappes located northwards [51,114,124]. The tectonic control on the sedimentation exerted by the NE-trending faults continued also during the Paleocene–Middle Eocene, as testified by the presence of deep-sea deposits of this age on top of the Late Cretaceous flysch (Sarca di Campiglio Member; [28]). Similar indications are provided by the presence of a NE-trending horst, controlling the deposition of Eocene platform carbonates, located between the Garda Lake and the Adige Valley and by two NNW–NNE and NNE–SSW trending grabens in the Lessini area, located East of the Adige Valley (Figure 13a) [125,126]. Eocene horst and graben structures display a width of about 10 km and the bounding faults are characterized by a maximum throw of some hundreds of meters.
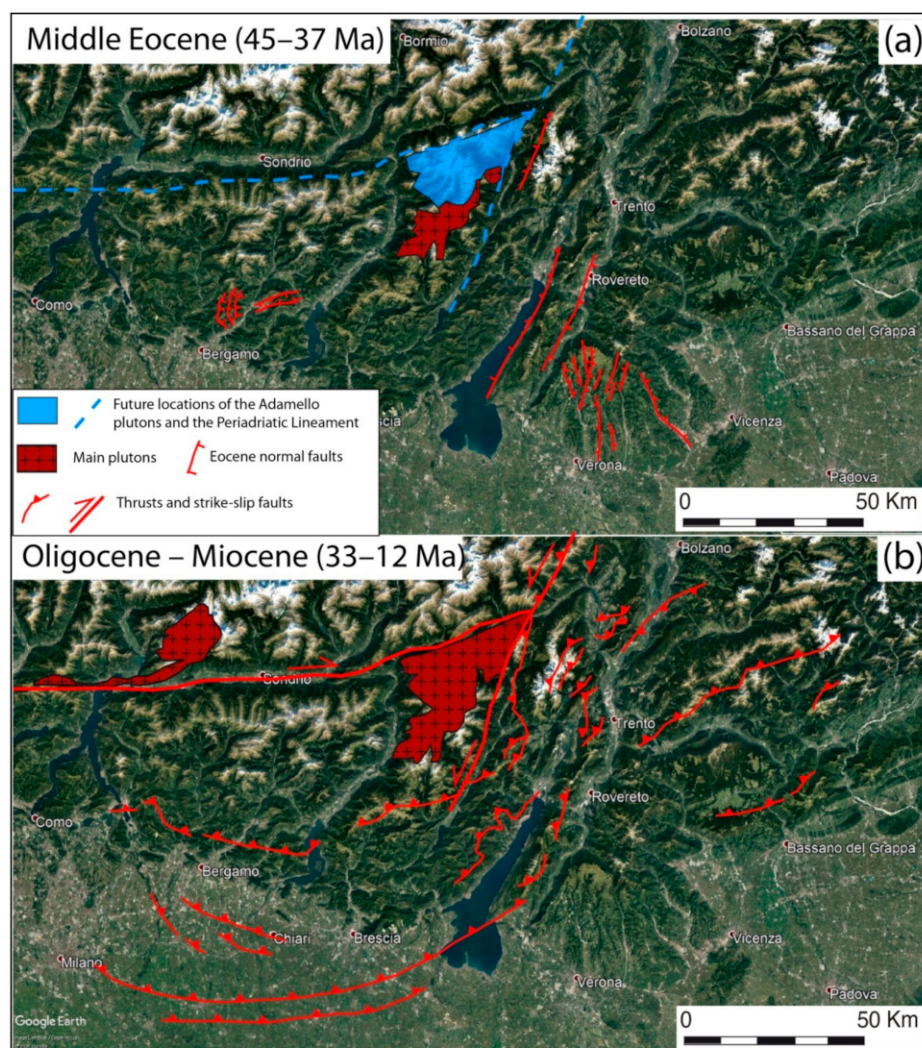
Figure 13. (**a**) Active faults and geodynamic setting in the Southern Alps during Middle Eocene time. (**b**) Active faults and geodynamic setting in the Southern Alps during Oligocene–Miocene times. Satellite imagery from Landsat/Copernicus dataset, Google Earth Pro.

5.4. Relation between Tectonics and Magmatism during Eocene–Oligocene

Intrusion of the Adamello batholith occurred in two phases during the tectonic evolution of the Southalpine/Austroalpine realm: the first took place during the period of extension which characterized the Southern Alps during the Middle Eocene (Figure 13a); the second, during the Late Eocene–Oligocene, when contraction and transpression localized along the Periadriatic Lineament (Figure 13b) [3,122,123,127]; The first phase took place during Lutetian/Bartonian times when Re di Castello and Corno Alto plutons were emplaced along the South Giudicarie Fault. Calc-alkaline dykes emplaced during the same time interval along normal faults in the Central Southern Alps [11]. Mafic dykes and apophyses intruded East of the present-day South Giudicarie Fault [13] and were accompanied by coeval volcaniclastic rocks exposed East of the Giudicarie Fault System, [13,128]. Basaltic volcanism since the Paleocene–Lower Eocene time is also well known in the Adige Valley and in the Lessini area [126,129–131]. In both cases, volcanism appears to be controlled by NNE- or NNW-trending normal faults of Eocene age (Figure 13a).

During the second phase, an extensive orogenic magmatism affected the Alpine chain, slightly postdating the final stages of Europe–Adria continental collision, accomplished at ~35–32 Ma [132]. Products of the alpine magmatism are mainly exposed in the vicinity of the Periadriatic Lineament. This magmatism comprises plutons, mafic-to-felsic dykes and volcanoclastic sequences. Plutonic bodies such as Traversella, Biella, Bergell and Riesen-

ferner are made up of diorite-tonalite-granodiorite rock associations with calc-alkaline (CA) to high-K calc- (HKCA) to shoshonitic compositions [133–135], mostly emplaced in a narrow timespan (33–29 Ma); the sole Traversella started intruding at 42 Ma [136]. Bergell and Riesenferner are in contact with the Periadriatic Lineament and alsoexhibit pervasive magmatic foliations often parallel to subparallel to the Periadriatic Lineament, calling for a syntectonic intrusion of these bodies [3]. A Periadriatic Lineament-parallel striking foliation has also been observed in the northernmost plutons of the Adamello batholith (the Avio and Presanella plutons), emplaced between 35 and 31 Ma [7,21]. This foliation is continuous throughout both units, witnessing a 4 Ma-long tectonic activity along the Periadriatic Lineament. A similar tectono-magmatic relation is shown by sheeted tonalite bodies ("lamellae") cropping out along the North Giudicarie Fault between Dimaro and Rumo, showing late Eocene to Oligocene age Rb/Sr and U/Pb ages [54,55]. Oligocene magmatism also includes a series of dykes occurring from the Western to the Eastern Alps, mainly consisting of calc-alkaline to shoshonitic rocks ranging from basalts and basaltic andesites to andesites, with some ultrapotassic lamproites outcropping within the Sesia–Lanzo Zone [137–139]. Most of the Oligocene dykes crop out inside a 20 km wide belt extending along the Periadriatic Lineament, suggesting that the latter acted as a feeder channel during this magmatic event [3,46]. Volcanism of Oligocene age is documented by the presence of a considerable number of andesitic clasts in flysch deposits from the Helvetic–Dauphinois of the External Western and Central Alps [140]. U/Pb zircon ages of 30–34 Ma has been observed for Haute Savoie and Taveyanne area samples, whereas U/Pb zircon age determinations for Glarus area (Northern Central Alps) has yielded two distinct clusters of Late Eocene/Early Oligocene (41–33 Ma) and Oligocene (33–29 Ma) age, respectively [140].

5.5. Emplacement of the Corno Alto Pluton

The intrusion depth of MOD is suggested at 10–15 km (3.5–5 kbar), as indicated by Al-in-Hbl barometry performed on ADA and RDC tonalites wrapping MOD outcrops. The emplacement of the Corno Alto granitoid at relatively shallow crustal levels is indicated by apatite fission track data in the hypothesis of a "normal" geothermal [63]. The depth of intrusion of the northeastern Adamello bodies was estimated at about 2.5 kbar in the Sil zone of the thermal aureole [59,65]). The magmatic roots of the southern and eastern Adamello plutons are not exposed. Absence of a magmatic anisotropy or solid-state foliation in both mafic and felsic lithotypes of the Corno Alto-M. Ospedale area suggests passive intrusion of the granitoid magma [141]. This is confirmed by the presence of thermal fractures filled by crystal-rich melts in the wall rocks, indicating the activation of the stoping process, with collapse and partial melting of basement blocks into peripheral magma [67]. These and other similar structures were described in the surroundings of the coeval Re di Castello mafic bodies and tonalite by Brack [142] and John and Blundy [143] (References [144–148] are cited in the Supplementary Material). Moreover, ductile structures (S/C composite foliation, boudinage, Figure 5b) visible in the basement surrounding the Corno Alto granite are interpreted as pre-intrusive and therefore unrelated to magma emplacement [73,117]. Widespread evidence of passive intrusion, coupled with the overall orientation of the Re di Castello and Corno Alto plutons, indicates that both mafic rocks and granitoids emplaced in a NE-trending extensional/transtensional fault zone, parallel to the normal faults active during Eocene in the eastern Southern Alps between Garda Lake and Adige Valley.

6. Conclusions

The diorite, tonalite and trondhjemite rocks exposed in the Corno Alto-M. Ospedale area intruded west of the South Giudicarie Fault, within St-Grt bearing schists of Val Borzago and Val Seniciaga and Ctd-bearing schists of Val Rendena at a depth of about 10–15 km. This is consistent with contact mineral assemblages including Sil, And, Crd, Grt and Sp, and the local partial melting observed in the Corno Alto area. Successive

exhumation did not expose the mafic roots, but only the upper magmatic reservoirs. The intrusion took place during Eocene along N- and NE-trending faults, bordering the "future Adamello area" to the east, when the central and eastern Southern Alps were affected by extensional tectonics, which followed the Eo-Alpine contractional tectonics in the Austroalpine units of the Eastern Alps and in the Southern Alps.

Magmatic rocks of the Corno Alto-M. Ospedale area are calc-alkaline, hence typical of late-orogenic magmatism. They are comparable with melts obtained by fractional crystallization of mantle-derived magmas and partial melting of crustal lithologies. The most evolved rocksof Corno Alto have compositions that are intermediate between the model melts produced by crustal anatexis and fractional crystallization. A simple fractional crystallization of mafic parental magmas fails to reproduce the most differentiated rocks of the Corno Alto.These features suggest that both partial melting of crustal rocks and fractional crystallization of mafic magmas may have played a role in the formation of the felsic rocks from Corno Alto.Accordingly, Sr and εNd show that only the Southern Re di Castello gabbro reveals mantle affinity (εNd > 0), while rocks of the Corno Alto-M. Ospedale area display εNd $\leq$ 0 and medium ^{87}Sr/^{86}Sr values indicating crust assimilation.

The results of the fractional crystallization with starting compositions buffered by QFM at P of 4 kbar, with 4% H_2O for four selected parental magmas produced Ol, Opx and Hbl for all samples and late Bt at late stage of crystallization. Some oxides, such as MgO, FeO and Na_2O, have trendssimilar to samples from Sostino (SOS) and Corno Alto Tonalite (CAT).

An attempt to model the crustal anatexis considered that the Adamello intruded the Southalpine crust and possibly the Alpine collisional wedge where both African and European units were represented. Samples from African and European lower and upper crust sections were considered as possible crustal contaminants. The calculated pseudosections obtained from different samples show that crustal melts were produced at deeper levels (6.5 to 10 kbar) with respect to the emplacement conditions.According to our thermodynamic model the most likely crustal contaminant is consistent with the European Lower Crust of the Serre Basement, Calabria (sample ELC1).

The intrusion of the eastern plutons of the Adamello batholith during Eocene is clearly correlated with the S-dipping Alpine subduction during Cretaceous time. In particular, the Eo-Alpine high-pressure event in the Eastern Alps, possibly connected with the S-directed subduction of a Tethyan oceanic remnant, is consistent with contamination of the Adriatic mantle since the Cretaceous time. The climax of the Eo-Alpine tectonics corresponded with collision in the Eastern Alps and S-directed thrusting in the Southern Alps. Later subduction of the Piedmont-Ligurian and Valais oceanic crust during Cretaceous-Eocene led to a period of tectonic quiescence/extension in the Southern Alps, which favored the evolution of the mantle-derived melts and their emplacement into extensional faults reactivating pre-existing discontinuities in the Adriatic crust. Final Alpine collision during Late Eocene–Oligocene times formed the Periadriatic lineament and favored the syn-tectonic emplacement of the central and northern Adamello tonalites under a contractional/transpressive tectonic regime.

Supplementary Materials: The following are available online at https://www.mdpi.com/article/10.3390/geosciences12010013/s1. Figure S1: Satellite view of the Adamello batholith with main peaks and valleys, comprising the main plutons and sample location. Figure S2: view of the Corno Alto massif with main peaks and valleys and sample location. Figure S3: SW view of the M. Ospedale area with main peaks and valleys and sample location. Figure S4: Satellite view of the Southern Re di Castello area with main peaks and valleys and sample location. Figure S5: (a) Stereoplot of the average Val Seniciaga basement foliation. (b) Basement foliation data: dip direction and dip. Figure S6: Panoramic view of Monte Ospedale. Figure S7: MCD (grey enclaves) dismembered by successive CAT intrusion on the rim of a minor MCD body near M.ga Campo. Figure S8: PCA analysis of Corno Alto-M. Ospedale mafic rocks amphiboles with classification diagram. Figure S9: PCA analysis of Corno Alto felsic samples. Figure S10: Harker diagrams for Corno Alto-M. Ospedale and Southern Re di Castello—M. Marser samples (a–h) Major element. (i–n) Trace elements and

REE. Figure S11: (a) SiO$_2$ vs. ^{87}Sr/^{86}Sr diagram for Corno Alto-M. Ospedale and Southern Re di Castello—M. Marser samples. (b) ^{87}Sr/^{86}Sr vs. εNd diagram for Corno Alto-M. Ospedale and Southern Re di Castello—M. Marser samples. Figure S12: Perple_X P-T pseudosections of ALC4 and CMP samples. Figure S13: Trace element patterns of average rock compositions from the study area normalized to the primitive mantle. Table S1: Location, description, mineralogy and geographic coordinates for Corno Alto–M. Ospedale, Re di Castello and M. Marser samples. Table S2: Major element compositions of Corno Alto–M. Ospedale, Re di Castello and M. Marser samples. Table S3: Trace elements and REE compositions of Corno Alto–M. Ospedale, Re di Castello, M. Marser samples. Table S4: Sr-Nd initial isotopic compositions for time of intrusion of the Corno Alto–M. Ospedale, Re di Castello and M. Marser samples. Table S5: Results of fractional crystallization modelling for sample 237 (Ulmer et al., 1985 [16]). Table S6: Results of fractional crystallization modelling for sample MK6 (MOD). Table S7: Results of fractional crystallization modelling for sample JM157 (Blundy and Sparks, 1992 [31]). Table S8: Results of fractional crystallization modelling for sample A3355 (MPD). Table S9: Mineral compositions of the Corno Alto-M. Ospedale mafic rockamphiboles. Table S10: Mineral compositions of ADA and RDC amphiboles for barometric calculations. Table S11: Molar % An-Ab-Or content of ADA and RDC Plagioclase and calculated P estimates for Amph-Pl pairs.

References

1. Callegari, E.; Brack, P. Geological Map of the Tertiary Adamello Batholith (Northern Italy). Explanatory Notes and Legend. *Mem. Sci. Geol. Padova.* **2002**, *54*, 19–49.
2. Laubscher, H.P. The late Alpine (Periadriatic) intrusions and the Insubric Line. *Mem. Soc. Geol. Ital.* **1983**, *26*, 21–30.
3. Rosenberg, C.L. Shear zones and magma ascent: A model based on a review of the Tertiary magmatism in the Alps. *Tectonics* **2004**, *23*, 1–21. [CrossRef]
4. Hansmann, W.; Oberli, F. Zircon inheritance in an igneous rock suite Implications for the pedogenesis of the southern Adamello batholith (Italian Alps). *Contrib. Mineral. Petrol.* **1991**, *107*, 501–518. [CrossRef]
5. Mayer, A.; Cortiana, G.; Dal Piaz, G.V.; Deleoule, E.; De Pieri, R.; Jobstraibizer, P. U-Pb single zircon ages of the Adamello batholith, Southern Alps. *Mem. Soc. Geol.* **2003**, *55*, 151–167.
6. Schaltegger, U.; Brack, P.; Ovtcharova, M.; Peytcheva, I.; Schoene, B.; Stracke, A.; Marocchi, M.; Bargossi, G.M. Zircon and titanite recording 1.5 million years of magma accretion, crystallization and initial cooling in a composite pluton (southern Adamello batholith, Northern Italy). *Earth Plan. Sci. Lett.* **2009**, *286*, 208–218. [CrossRef]
7. Schaltegger, U.; Nowak, A.; Ulianov, A.; Fischer, C.M.; Gerdes, A.; Spikings, R.; Whitehouse, M.J.; Bindeman, I.; Hanchar, J.M.; Duff, J.; et al. Zircon Petrochronology and ^{40}Ar/^{39}Ar Thermochronology of the Adamello Intrusive Suite, N. Italy: Monitoring the Growth and Decay of an Incrementally Assembled Magmatic System. *J. Petrol.* **2019**, *60*, 701–722. [CrossRef]
8. Del Moro, A.; Ferrara, G.; Tonarini, S.; Callegari, E. Rb-Sr systematics on rocks from the Adamello batholith. *Mem. Soc. Geol.* **1983**, *26*, 261–284.

9.   Sciunnach, D.; Borsato, A. Plagioclasearenites in the Molveno Lake area (Trento): Record of an Eocene volcanic arc. *Studi Trentini Sci. Nat.* **1994**, *69*, 81–92.

10.   Fantoni, R.; Bersezio, R.; Forcella, F.; Gorla, L.; Mosconi, A.; Picotti, V. New dating of the tertiary magmatic products of the central Southern Alps, bearings on the interpretation of the Alpine tectonic history. *Mem. Soc. Geol.* **1999**, *51*, 47–61.

11.   D'Adda, P.; Zanchi, A.; Bergomi, M.; Berra, F.; Malusà, M.G.; Tunesi, A.; Zanchetta, S. Polyphase thrusting and dyke emplacement in the central Southern Alps (Northern Italy). *Int. J. Earth Sci.* **2010**, *100*, 1095–1113. [CrossRef]

12.   Bartoli, O.; Meli, S.; Bergomi, M.; Sassi, R.; Magaraci, D.; Lyu, D.-Y. Geochemistry and zircon U-Pb geochronology of magmatic enclaves in trachytes from the Euganean Hills (NE Italy): Further constraints on Oligocene magmatism in the eastern Southern Alps. *Eur. J. Mineral.* **2015**, *27*, 161–174. [CrossRef]

13.   Martin, S.; Macera, P. Tertiary volcanism in the Italian Alps (Giudicarie fault zone, NE Italy): Insight for double alpine magmatic arc. *Ital. J. Geosci.* **2014**, *133*, 63–84. [CrossRef]

14.   Brombin, V.; Bonadiman, C.; Jourdan, F.; Roghi, C.; Coltorti, M.; Webb, L.E.; Callegaro, S.; Bellieni, G.; De Vecchi, G.; Sedea, R.; et al. Intraplate magmatism at a convergent plate boundary: The case of the Cenozoic northern Adria magmatism. *Earth. Sci. Rev.* **2019**, *192*, 355–378. [CrossRef]

15.   Del Moro, A.; Dal Piaz, G.V.; Martin, S.; Venturelli, G. Dati radiometrici e geochimici preliminari su magmatiti oligoceniche del settore meridionale del massiccio Ortles-Cevedale. *Rend. Soc. Geol. Ital.* **1981**, *4*, 265–266.

16.   Ulmer, P.; Callegari, E.; Sonderegger, U.C. Genesis of the mafic and ultramafic rocks and their genetical relations to the tonalitic-trondhjemitic granotoids of the southern part of the Adamello batholith, (Northern Italy). *Mem. Soc. Geol.* **1983**, *26*, 171–222.

17.   Nandedkar, R.H.; Ulmer, P.; Müntener, H. Fractional crystallization of primitive, hydrous arc magmas: An experimental study at 0.7 GPa. *Contrib. Mineral. Petrol.* **2014**, *167*, 1–27. [CrossRef]

18.   Borsi, S.; Callegari, E.; Del Moro, A.; Ferrara, G.; Fratta, M.; Giuliani, O.; Macera, P.; Pardini, G.; Pescia, A.; Tonarini, S. Geochronological investigations on the Adamello-Presanella massif. In Proceedings of the 5th ECOG, Pisa, Italy, 5–10 September 1977.

19.   Cortecci, G.; Del Moro, A.; Leone, G.; Pardini, G. Correlation between Strontium and Oxygen isotopic compositions of rocks from the Adamello massif (northern Italy). *Contrib. Mineral. Petrol.* **1979**, *68*, 421–427. [CrossRef]

20.   Juteau, M.; Michard, A.; Albarede, F. The Pb-Sr-Nd isotope geochemistryof some recent circum Mediterranean granites. *Contrib. Mineral. Petrol.* **1986**, *92*, 331–340. [CrossRef]

21.   Del Moro, A.; Pardini, G.; Quercioli, C.; Villa, I.M.; Callegari, E. Rb/Sr and K/Ar chronology of the Adamello granotoids, Southern Alps. *Mem. Soc. Geol.* **1983**, *26*, 285–301.

22.   Macera, P.; Ferrara, G.; Pescia, A.; Callegari, E. A geochemical study on the acid and basic rocks of the Adamello batholith. *Mem. Soc. Geol.* **1983**, *26*, 223–259.

23.   Thompson, A.B.; Matile, L.; Ulmer, P. Some thermal constraints on crustal assimilation during fractionation of hydrous, mantle-derived magmas with examples from Central Alpine Batholiths. *J. Petrol.* **2002**, *43*, 403–422. [CrossRef]

24.   Bigazzi, G.; Del Moro, A.; Macera, P. A quantitative approach to trace element and Sr isotope evolution in the Adamello batholith (northern Italy). *Contrib. Mineral. Petrol.* **1986**, *94*, 46–53. [CrossRef]

25.   Ulmer, P. Mantle petrogenesis of calc-alcaline parental magmas: Experimental constraints and petrologic evidence from the Adamello granitoids. In Proceedings of the IV Summer School, Siena, Italy, 23 September–7 October 1992; pp. 95–114.

26.   Macera, P.; Del Moro, A.; Martin, S.; Pieroni, M.; Tambellini, K. The role of the lower crust on the genesis of mafic and felsic rocks from the Adamello batholith (Southern Alps); geochemical and isotope (Sr-Nd) evidence. *Mem. Soc. Geol.* **1998**, *50*, 74–77.

27.   Castellarin, A.; Dal Piaz, G.V.; Picotti, V.; Selli, L.; Cantelli, L.; Martin, S.; Montresor, L.; Rigatti, G.; Prosser, G.; Bollettinari, G.; et al. Note Illustrative della Carta Geologica d'Italia Alla Scala 1:50,000, Sheet n. 059, Tione di Trento. Provincia Autonoma di Trento. 2005. Available online: https://www.researchgate.net/publication/235420167_Note_illustrative_della_Carta_Geologica_d%27Italia_alla_scala_150000_Foglio_059_Tione_di_Trento (accessed on 15 October 2021).

28.   Dal Piaz, G.V.; Castellarin, A.; Martin, S.; Selli, L.; Carton, A.; Pellegrini, G.B.; Casolari, E.; Daminato, F.; Montresor, L.; Picotti, V.; et al. Note Illustrative della Carta Geologica d'Italia Alla Scala 1:50,000, Sheet n.042 Malé. Provincia Autonoma di Trento. 2007. Available online: https://www.researchgate.net/publication/235420138_Note_illustrative_della_Carta_Geologica_d%27Italia_alla_scala_150000_Foglio_042_Male (accessed on 15 October 2021).

29.   Callegari, E.; Dal Piaz, G.V.; Gatto, G. *Carta Geologica del Gruppo Adamello-Presanella*; Consiglio Nazionale delle Ricerche: Rome, Italy, 1998.

30.   Whitney, D.L.; Evans, B.W. Abbreviations for names of rock-forming minerals. *Am. Miner.* **2009**, *95*, 185–187. [CrossRef]

31.   Blundy, J.D.; Sparks, R.S.J. Petrogenesis of mafic inclusion in granitoids of the Adamello Massif. *J. Petrol.* **1992**, *33*, 1039–1104. [CrossRef]

32.   Gualda, G.A.; Ghiorso, M.S.; Lemons, R.V.; Carley, T.L. Rhyolite-MELTS: A modified calibration of MELTS optimized for silica-rich, fluid bearing magmatic systems. *J. Petrol.* **2012**, *53*, 875–890. [CrossRef]

33.   Gualda, G.A.; Ghiorso, M.S. MELTS-Excel: A Microsoft Excel-based MELTS interface for research and teaching of magma properties and evolution. *Geochem. Geophys. Geosyst.* **2015**, *16*, 315–324. [CrossRef]

34.   Connolly, J.A.D. The geodynamic equation of state: What and how. *Geochem. Geophys. Geosyst.* **2009**, *10*, Q10014. [CrossRef]

35.   Holland, T.J.B.; Powell, R. An improved and extended internally consistent thermodynamic dataset for phases of petrological interest, involving a new equation of state for solids. *J. Metamorp. Geol.* **2011**, *29*, 333–383. [CrossRef]

36. Caggianelli, A.; Rottura, A.; Pinarelli, L. Lower crustal granite genesis connected with chemical fractionation in the continental crust of Calabria (Southern Italy). *Eur. J. Mineral.* **1991**, *3*, 159–180. [CrossRef]

37. Giobbi Origoni, E.; Gregnanin, A. The crystalline basement of the "Massiccio delle tre valli Bresciane": New petrographic and chemical data. *Mem. Soc. Geol.* **1983**, *26*, 133–144.

38. Voshage, H.; Hofmann, A.W.; Mazzucchelli, M.; Rivalenti, G.; Sinigoi, S.; Raczek, I.; Demarchi, G. Isotopic evidence from the Ivrea Zone for a hybrid lower crust formed by magmatic underplating. *Nature* **1990**, *347*, 731–736. [CrossRef]

39. White, R.W.; Powell, R.; Holland, T.J.B.; Johnson, T.E.; Green, E.C.R. New mineral activity–composition relations for thermodynamic calculations in metapelitic systems. *J. Metamorp. Geol.* **2014**, *32*, 261–286. [CrossRef]

40. White, R.W.; Powell, R.; Johnson, T.E. The effect of Mn on mineral stability in metapelites revisited: New *a–x* relations for manganese-bearing minerals. *J. Metamorp. Geol.* **2014**, *32*, 809–828. [CrossRef]

41. White, R.W.; Powell, R.; Holland, T.J.B.; Worley, B.A. The effect of TiO_2 and Fe_2O_3 on metapelitic assemblages at greenschist and amphibolite facies conditions: Mineral equilibria calculations in the system K_2O–FeO–MgO–Al_2O_3–SiO_2–H_2O–TiO_2–Fe_2O_3. *J. Metamorp. Geol.* **2000**, *18*, 497–511. [CrossRef]

42. Holland, T.J.B.; Powell, R. Activity–composition relations for phases in petrological calculations: An asymmetric multicomponent formulation. *Contrib. Mineral. Petrol.* **2003**, *145*, 492–501. [CrossRef]

43. Green, E.C.R.; White, R.W.; Diener, J.F.A.; Powell, T.J.B.; Palin, R.M. Activity–composition relations for the calculation of partial melting equilibria in metabasic rocks. *J. Metamorp. Geol.* **2016**, *34*, 845–869. [CrossRef]

44. Salomon, W. Über das Alter, Lagerungsform und Entstehungsart der periadriatichengranitischkörnigenMassen. *Tschermaks Mitt.* **1897**, *17*, 109–284.

45. Exner, C. Die geologische Position der Magmatitedes penadriatischen Lineamentes. *Verh. Geol. B-A Wien.* **1976**, *2*, 3–64.

46. Stipp, M.; Fügenschuh, B.; Gromet, L.; Stünitz, H.; Schmid, S. Contemporaneous plutonism and strike-slip faulting: A case study from the Tonale fault zone north of the Adamello pluton (Italian Alps). *Tectonics* **2004**, *23*, TC3004. [CrossRef]

47. Prosser, G. Strike-slip movements and thrusting along a transpressive fault zone: The North Giudicane line (Insubric Line, Northern Italy). *Tectonics* **1998**, *17*, 921–937. [CrossRef]

48. Viola, G.; Mancktelow, N.S.; Seward, D. Late Oligocene-Neogene evolution of Europe-Adria collision: New structural and geochronological evidence from the Giudicarie fault system (Italian Eastern Alps). *Tectonics* **2001**, *20*, 999–1020. [CrossRef]

49. Cassinis, G.; Perotti, C.R. Interazione strutturale permiana tra la Linea delle Giudicarie e i bacini di Collio, Tione e Tregiovo. *Boll. Soc. Geol.* **1993**, *112*, 1021–1036.

50. Bertotti, G.; Picotti, V.; Bernoulli, D.; Castellarin, A. From rifting to drifting: Tectonic evolution of the South-Alpine upper crust from the Triassic to the Early Cretaceous. *Sediment. Geol.* **1993**, *86*, 53–76. [CrossRef]

51. Castellarin, A.; Piccioni, S.; Prosser, G.; Sanguinetti, E.; Sartori, R.; Selli, L. Mesozoic continental riftng and Neogene inversion along the South Giudicarie Line (NE Brenta Dolomites). *Mem. Soc. Geol.* **1993**, *49*, 125–144.

52. Castellarin, A. Evoluzione paleotettonica sinsedimentaria del limite tra "piattaforma veneta" e "bacino lombardo" a Nord di Riva del Garda. *Giorn. Geol.* **1972**, *38*, 11–212.

53. Castellarin, A.; Fesce, A.; Picotti, V.; Pini, G.A.; Prosser, G.; Sartori, R.; Selli, L.; Cantelli, L.; Ricci, R. Structural and kinematic analyses of the Giudicarie deformation belt. Implications for compressional tectonics of Southern Alps. *Miner. Petrogr. Acta* **1988**, *30*, 287–310.

54. Martin, S.; Prosser, G.; Morten, L. Tectono-magmatic evolution of sheeted plutonic bodies along the North Giudicarie Line (northern Italy). *Geol. Rund.* **1993**, *82*, 51–66. [CrossRef]

55. Pomella, H.; Klötzli, U.; Scholger, R.; Stipp, M.; Fügenschuh, B. The Northern Giudicarie and the Meran–Mauls fault (Alps, Northern Italy) in the light of new paleomagnetic and geochronological data from boudinaged Eo-/Oligocene tonalites. *Int. J. Earth Sci.* **2011**, *100*, 1827–1850. [CrossRef]

56. Salomon, W. Die Adamellogruppe, Teil I. *Abhandl. Geol. Reichsants.* **1908**, *21*, 1–433.

57. Trener, G.B. Età e giacitura del massiccio granitico del Corno Alto (Adamello). *Tridentum* **1911**, *13*, 1–14.

58. Locardi, E. Il Monte Ospedale (Adamello Centrale). Studio Geologico-Petrografico. Master's Thesis, University of Padova, Padua, Italy, 1958.

59. Boriani, A.; Giobbi Origoni, E. Heat transfer in the thermo-metamorphic aureola of the north-eastern sector of Mt. Adamello. *Rend. SIMP* **1982**, *38*, 1351–1360.

60. Zanettin, B.; Justin Visentin, E. Genesi di cornubianiti a granato, andalusite e cordierite nell'aureola di contatto dell'Adamello. *St. Trent. Sci. Nat.* **1968**, *45*, 224–245.

61. Tornielli, V. Studio Geologico e Geochimico dei Corpi Basici della Val Seniciaga, Massiccio dell'Adamello. Master's Thesis, University of Padova, Padua, Italy, 1995.

62. Bazzolo, F. Studio Geologico e Strutturale dei Corpi Magmatici e del Basamento Cristallino della Val Seniciaga, Massiccio dell'Adamello. Master's Thesis, University of Padova, Padua, Italy, 1995.

63. Martin, S.; Bigazzi, G.; Zattin, M.; Viola, G.; Balestrieri, M.G. Neogene kinematics of the Giudicarie Fault (Central-Eastern Alps, Italy): New apatite fission-track data. *Terra Nova* **1998**, *10*, 217–221. [CrossRef]

64. Spalla, M.I.; Zanoni, D.; Gosso, G.; Zucali, M. Deciphering the geologic memory of a Permian conglomerate of the Southern Alpsby pebble P–T estimates. *Int. J. Earth Sci.* **2009**, *98*, 203–226. [CrossRef]

65. Rossi, J.N. Metamorfismo di contatto sugli scisti del versante sinistro di Val Borzago. *Atti Mem. Acc. Patavina Sci. Lett. Arti. Cl. Sc. Mat. Nat.* **1969**, *81*, 329–353.
66. Giorio, C.L. Studio Geologico del Basamento Cristallino della Val Rendena. Master's Thesis, University of Padova, Padua, Italy, 1995.
67. Marsh, B.D. On the mechanics of igneous diapirism, stoping, and zone melting. *Am. J. Sci.* **1982**, *282*, 808–855. [CrossRef]
68. Salomon, W. Die Adamellogruppe, Teil II. *Abhandl. Geol. Reichsants.* **1910**, *21*, 435–603.
69. Bianchi, A.; Dal Piaz, G.B. Il problema dell'età del Corno Alto nel massiccio dell'Adamello. *Mem. Soc. Geol. Univ. Padova* **1950**, *16*, 1–12.
70. Colbertaldo, D. Ricerche geológico-petrografiche sul settore orientale dell'Adamello fra Val di Genova e Val di Breguzzo. *Mem. Ist. Geol. Univ. Padova* **1942**, *14*, 1–44.
71. Zattin, M. Studio Geologico del Plutone del Corno Alto, Batolite dell'Adamello. Master Thesis, University of Padova, Padua, Italy, 1994.
72. Bianchi, A.; Callegari, E.; Jobstraibizer, P.G. I tipi petrografici fondamentali del plutone dell'Adamello (tonaliti, quarzodioriti, granodioriti, e loro varietà leucocrate). *Mem. Ist. Geol Min. Univ. Padova.* **1970**, *27*, 1–148.
73. Zattin, M.; Bazzolo, F.; Giorio, L.; Martin, S.; Tornielli, V. Intrusioni multiple nell'area del Corno Alto, Massiccio dell'Adamello. *Atti Tic. Sc. Terra* **1995**, *3*, 45–56.
74. De Pieri, R.; Jobstraibizer, P.G. Cryslal chemistry of biotites from dioritic to granodioritic rock-types of Adamello Massif (Northern ltaly). *N. Jb. Miner. Abh.* **1983**, *148*, 58–82.
75. Bellieni, G.; Cavazzini, G.; Fioretti, A.M.; Visentin, E.J.; Zanettin, B.; Zantedeschi, P. Magmatic evolution of the Borzago Valley calc-alkaline basic satellite body (Southern Adamello batholith-Northern Italy) and role of xenocrystic phases in its geochemistry. *Eur. J. Mineral.* **1995**, *7*, 967–988. [CrossRef]
76. Mutch, E.J.F.; Blundy, J.D.; Tattich, B.C.; Cooper, F.J.; Booker, R.A. An experimental study of amphibole stability in low-pressure granitic magmas and a revised Al-in-Hornblende geobarometer. *Contrib. Mineral. Petrol.* **2016**, *171*. [CrossRef]
77. Barker, F. Trondhjemite: Definition, environment and hypotheses of origin. In *Trondhjemites, Dacites, and Related Rocks*, 1st ed.; Elsevier: New York, NY, USA, 1979; pp. 1–12.
78. Frost, B.R.; Frost, C.D. A geochemical classification fro feldspathic igneous rocks. *J. Petrol.* **2008**, *49*, 1955–1969. [CrossRef]
79. Daly, R.A. The geology of Ascension Island. *Proc. Am. Acad. Arts. Sci.* **1925**, *60*, 1–80. [CrossRef]
80. von Blanckenburg, F.; Kagami, H.; Deutsch, A.; Oberli, F.; Meier, M.; Wiedenbeck, M.; Barth, S.; Fischer, H. The origin of the Alpine plutons along the Periadriatic lineament. *Schweiz. Mineral. Petrogr. Mitt.* **1998**, *78*, 55–66.
81. Doštal, J.; Dupuy, C.; Leyreloup, A. Geochemistry and petrology of meta-igneous granulitic xenoliths in neogene volcanic rocks of the massif central, France-implicationsfor the lower crust. *Earth Planet. Sci. Lett.* **1980**, *50*, 31–40. [CrossRef]
82. Kempton, P.D.; Downes, H.; Embey-Isztin, A. Mafic Granulite Xenoliths in Neogene Alkali Basalts from the Western Pannonian Basin: Insights into the Lower Crust of a Collapsed Orogen. *J. Petrol.* **1997**, *38*, 941–970. [CrossRef]
83. Loock, G.; Stosch, H.-G.; Seck, H.A. Granulite facies lower crustal xenoliths from the Eifel, West Germany: Petrological and geochemical aspects. *Contrib. Mineral. Petrol.* **1990**, *105*, 25–41. [CrossRef]
84. Coward, M.P.; Dietrich, D.; Park, R.G. Alpine tectonics. *Geol. Soc. Spec. Publ.* **1989**, *45*, 1–29. [CrossRef]
85. Langone, A.; Gueguen, E.; Prosser, G.; Caggianelli, A.; Rottura, A. The Curinga-Girifalco fault zone (Northern Serre, Calabria) and its significance within the Alpine tectonic evolution of the western Mediterranean. *J. Geodyn.* **2006**, *42*, 140–158. [CrossRef]
86. Heymes, T.; Bouillin, J.-P.; Pécher, A.; Monié, P.; Compagnoni, R. Middle Eocene extension in the Mediterranean Calabro-Peloritan belt (southern Italy): Insights from the Aspromonte nappes pile. *Tectonics* **2008**, *27*, TC2006. [CrossRef]
87. Cirrincione, R.; Fazio, E.; Fiannacca, P.; Ortolano, G.; Pezzino, A.; Punturo, R. The Calabria-Peloritani Orogen, a composite terrane in Central Mediterranean; its overall architecture and geodynamic significance for a pre-Alpine scenario around the Tethyan basin. *Period. Mineral.* **2015**, *84*, 701–749. [CrossRef]
88. Schenk, V. P-T-t path of the lower crust in the Hercynian fold belt of Southern Calabria. *Geol. Soc. Spec. Publ.* **1989**, *43*, 337–342. [CrossRef]
89. Henk, A.; Leander, F.; Teufel, S.; Oncken, O. Magmatic Underplating, Extension, and Crustal Reequilibration: Insights from a Cross-Section through the Ivrea Zone and Strona-Ceneri Zone, Northern Italy. *J. Geol.* **1997**, *105*, 367–377. [CrossRef]
90. Tiepolo, M.; Tribuzio, R.; Langone, A. High-Mg andesite petrogenesis by amphibole crystallization and Ultramafic crust assimilation: Evidence from Adamello hornblendites (Central Alps, Italy). *J. Petrol.* **2011**, *52*, 1011–1045. [CrossRef]
91. Beard, J.S.; Lofgren, G.E. Dehydration melting and water-saturated melting of basaltic and andesitic greenstones and amphibolites at 1, 3 and 6–9 kb. *J. Petrol.* **1991**, *32*, 365–401. [CrossRef]
92. Patiño Douce, A.E.; Beard, J.S. Dehydration melting of biotite gneiss and quartz amphibolite from 3 to 15 kbar. *J. Petrol.* **1995**, *36*, 707–738. [CrossRef]
93. Vielzeuf, D.; Holloway, J.R. Experimental determination of the fluid-absent melting relations in the pelitic system–consequences for crustal differentiation. *Contrib. Mineral. Petrol.* **1988**, *98*, 257–276. [CrossRef]
94. Clemens, J.D.; Vielzeuf, D. Constraints on melting and magma formation in the crust. *Earth Planet. Sci. Lett.* **1987**, *86*, 287–306. [CrossRef]
95. Bartoli, O.; Carvalho, B.B. Anatectic granites in their source region: A comparison between experiments, thermodynamic modelling and nanogranitoids. *Lithos* **2021**, 106046. [CrossRef]

96. Van Hinsbergen, J.J.D.; Torsvik, T.H.; Schmid, S.M.; Matenço, L.C.; Maffione, M.; Vissers, R.L.M.; Gürer, D.; Spakman, W. Orogenic architecture of the Mediterranean region and kinematic reconstruction of its tectonic evolution since the Triassic. *Gondwana Res.* **2020**, *81*, 79–229. [CrossRef]

97. Thöni, M. Sm–Nd isotope systematics in garnet from different lithologies (Eastern Alps): Age results, and an evaluation of potential problems for Sm–Nd garnet chronometry. *Chem. Geol.* **2002**, *185*, 255–281. [CrossRef]

98. Thöni, M. Dating eclogite-facies metamorphism in the Eastern Alps–approaches, results, interpretations: A review. *Mineral. Petrol.* **2006**, *88*, 123–148. [CrossRef]

99. Sölva, H.; Grasemann, B.; Thöni, M.; Habler, G. The eo-Alpine high-pressure belt in the Eastern Alps: A kinematic exhumation model and its tectonic implications. *Mitt. Osterr. Miner. Ges.* **2005**, *150*, 147.

100. Schmid, S.M.; Scharf, A.; Handy, M.R.; Rosenberg, C.L. The Tauern Window (Eastern Alps, Austria): A new tectonic map, with cross-sections and a tectonometamorphic synthesis. *Swiss J. Geosci.* **2013**, *106*, 1–32. [CrossRef]

101. Miller, C. Chemismus und phasenpetrologische Untersuchungen der Gesteine aus der Eklogitzone des Taurenfenesters, Osterreich. *Tschermaks Min. Petr. Mitt.* **1977**, *24*, 221–277. [CrossRef]

102. Holland, T.J.B. High water activities in the generation of high pressure kyanite eclogites of the Tauern Window, Austria. *J. Geol.* **1979**, *87*, 1–27. [CrossRef]

103. Wagreich, M. Subduction tectonic erosion and Late Cretaceous subsidence along the northern Austroalpine margin (Eastern Alps, Austria). *Tectonophysics* **1995**, *242*, 63–78. [CrossRef]

104. Kurz, W.; Handler, R.; Bertoldi, C. Tracing the exhumation of the Eclogite Zone (Tauern Window, Eastern Alps) by ^{40}Ar/^{39}Ar dating of white mica in eclogites. *Swiss J. Geosci.* **2008**, *101*, 191–206. [CrossRef]

105. Frisch, W. Tectonic progradation and plate tectonic evolution of the Alps. *Tectonophysics* **1979**, *60*, 121–139. [CrossRef]

106. Schmid, S.M.; Fügenschuh, B.; Kissling, E.; Schuster, R. Tectonic map and overall architecture of the Alpine orogen. *Eclogae Geol. Helv.* **2004**, *97*, 93–117. [CrossRef]

107. Trümpy, G. Penninic-Austroalpine boundary in the Swiss Alps: A continental margin and its problems. *Am. J. Sci.* **1975**, *275A*, 209–238.

108. Miller, C. On the metamorphism of eclogites and high-grade blueschists from the Penninic Terrane of the Tauern Window, Austria. *Schweiz Mineral. Petrogr. Mitt.* **1974**, *54*, 371–384.

109. Dingeldey, C.; Dallmeyer, L.D.; Koller, F.; Massonne, H.-J. P-T t history of the Lower Austroalpine Nappe Complex NW of the Tauern Window: Implications for the geotectonic evolution of the central Eastern Alps. *Contrib. Miner. Petrol.* **1997**, *129*, 1–19. [CrossRef]

110. Wiederkehr, M.; Bousquet, R.; Schmid, S.M.; Berger, A. From subduction to collision: Thermal overprint of HP/LT meta-sediments in the north-eastern Lepontine Dome (Swiss Alps) and consequences regarding the tectono-metamorphic evolution of the Alpine orogenic wedge. *Swiss J. Geosci.* **2008**, *101*, 127–155. [CrossRef]

111. Wiederkehr, M.; Sudo, M.; Bousquet, R.; Berger, A.; Schmid, S.M. Alpine orogenic evolution from subduction to collisional thermal overprint: The ^{40}Ar/^{39}Ar age constraints from the Valaisan Ocean, central Alps. *Tectonics* **2009**, *28*, 1–28. [CrossRef]

112. Lippitsch, R.; Kissling, E.; Ansorge, J. Upper mantle structure beneath the Alpine orogen from high-resolution teleseismic tomography. *J. Geophys. Res.* **2003**, *108*, 2376. [CrossRef]

113. Kissling, E.; Schmid, S.M.; Lippitsch, R.; Ansorge, J.; Fügenschuh, B. Lithosphere structure and tectonic evolution of the Alpine arc: New evidence from high-resolution teleseismic tomography. *Geol. Soc. Lond. Mem.* **2006**, *32*, 129–145. [CrossRef]

114. Doglioni, C.; Bosellini, A. Eoalpine and mesoalpine tectonics of the Southern Alps. *Geol. Rund.* **1987**, *76*, 735–754. [CrossRef]

115. Bersezio, R.; Fornaciari, M.; Gelati, R.; Napolitano, A.; Valdistrulo, A. The significance of the Upper Cretaceous to Miocène clastic wedges in the déformation history of the Lombardian southern Alps. *Geol. Alp.* **1993**, *69*, 3–20.

116. Zanchetta, S.; D'Adda, P.; Zanchi, A.; Barberini, A.; Villa, I.M. Cretaceous-Eocene compression in the central Southern Alps (N Italy) inferred from ^{40}Ar/^{39}Ar dating of pseudotachylytes. *J. Geodyn.* **2011**, *51*, 245–263. [CrossRef]

117. Brack, P. Structures in the southwestern border of the Adamello intrusion. *Schweiz Mineral. Petrogr. Mitt.* **1981**, *61*, 37–50.

118. Brack, P. Geologie der Intrusiva und Nebengensteine des Südwest-Adamello (Nord-Italian). Ph.D. Thesis, Eidgenössische Technische Hochschule Zürich, Zürich, Switzerland, 1984.

119. Brack, P.; Dal Piaz, G.V.; Baroni, C.; Carton, A.; Nardin, M.; Pellegrini, G.B.; Pennacchioni, G.; Monte Adamello, F. 058. Note Illustrative della Carta Geologica d'Italia e Carta Geologica Alla Scala 1:50,000. Provincia Autonoma di Trento. 2008. Available online: https://www.research-collection.ethz.ch/handle/20.500.11850/158778 (accessed on 15 October 2021).

120. Bernoulli, D.; Winkler, W. Heavy mineral assemblages from Upper Cretaceous South- and Austroalpine flysch sequences (Northern Italy and Southern Switzerland): Source terranes and palaeotectonic implications. *Eclogae Geol. Helv.* **1990**, *83*, 287–310.

121. Berra, F.; Carminati, E. Subsidence history from backstripping analysis of the Permo-Mesozoic succession of the Central Southern Alps (Northern Italy). *Basin Res.* **2009**, *22*, 952–975. [CrossRef]

122. Di Giulio, A.; Carrapa, B.; Fantoni, R.; Gorla, L.; Valdisturlo, A. Middle Eocene to Early Miocene sedimentary evolution of the western Lombardian segment of the South Alpine foredeep (Italy). *Int. J. Earth Sci.* **2001**, *90*, 534–548. [CrossRef]

123. Bersezio, R.; Fornaciari, M. Geometria e caratteri stratigrafici della Sequenza Cenomaniana nell'Bacino Lombardo (Alpi Meridionali). *Riv. Ital. Paleont. Strat.* **1988**, *94*, 425–454.

124. Castellarin, A.; Morten, L.; Bargossi, G.M. Conglomerati di conoide sottomarina nel flysch insubrico di Male' e Rumo (Trento). *Boll. Soc. Geol. Ital.* **1976**, *95*, 513–525.

125. Luciani, V. Stratigrafia sequenziale del Trentino nella catena del Monte Baldo (Provincia di Verona e Trento). *Mem. Sci. Geol.* **1989**, *41*, 263–351.

126. Zampieri, D. Tertiary extension in the Southern Trento Platform, Southern Alps, Italy. *Tectonics* **1995**, *14*, 645–657. [CrossRef]

127. Garzanti, E.; Malusà, M.G. The Oligocene Alps: Domal unroofing and drainage development during early orogenic growth. *Earth Planet. Sci. Lett.* **2008**, *268*, 487–500. [CrossRef]

128. Bars, H.; Grigoriadis, J. Ueber Basalttuffe des Oberen Mittel-Eozdns der Scaglia Grigia in Val di Non (Nonsberg), Provinz Trient, Italien. *Neues Jahrb. Geol. Palaon. Abh.* **1969**, *11*, 643–654.

129. Piccoli, G. Recenti ricerche geologiche sulle manifestazioni vulcaniche cretaceo-cenozoiche delle Venezie. *Boll. Serv. Geol.* **1962**, *82*, 79–108.

130. Castellarin, A.; Piccoli, G. *I Vulcani Eocenici nei Dintorni di Rovereto*; Museo Geologico Giovanni Cappellini: Bologna, Italy, 1966; p. 75.

131. Beccaluva, L.; Bianchini, G.; Bonadiman, C.; Coltorti, M.; Milani, L.; Salvini, L.; Siena, F.; Tassinari, R. Intraplate lithospheric and sublithospheric components in the Adriatic domain: Nephelinite to tholeiite magma generation in the Paleogene Veneto volcanic province, southern Alps. *Geol. Soc. Am. Spec. Pap.* **2007**, *418*, 131–152.

132. Handy, M.R.; Schmid, S.M.; Bousquet, R.; Kissling, E.; Bernoulli, D. Reconciling plate-tectonic reconstructions of Alpine Tethys with the geological–geophysical record of spreading and subduction in the Alps. *Earth Sci. Rev.* **2010**, *102*, 121–158. [CrossRef]

133. Bigioggero, B.; Colombo, A.; Del Moro, A.; Gregnanin, A.; Macera, P.; Tunesi, A. The Oligocene Valle del Cervo Pluton: An example of shoshonitic magmatism inthe Western Italian Alps. *Mem. Sci. Geol. Padova* **1994**, *46*, 409–421.

134. Zanoni, D.; Spalla, M.I.; Gosso, G. Structure and PTestimates across late-collisional plutons: Constraints on the exhumation of western Alpine continental HP units. *Int. Geol. Rev.* **2010**, *52*, 1244–1267. [CrossRef]

135. Zanoni, D.; Corti, L.; Roda, M. Cooling history of the Biellapluton and implication for Oligocene to Miocene tectonics of the Sesia-Lanzo Zone, Austroalpine, Western Alps. *Int. Geol. Rev.* **2021**. [CrossRef]

136. Ji, W.Q.; Malusà, M.G.; Tiepolo, M.; Langone, A.; Zhao, L.; Wu, F.Y. Synchronous Periadriatic magmatism in theWestern and Central Alps in the absence of slab breakoff. *Terra Nova* **2019**, *31*, 120–128. [CrossRef]

137. Dal Piaz, G.V.; Del Moro, A.; Martin, S.; Venturelli, G. Post-collisional magmatism in the Ortler-Cevedale Massif (Northern Italy). *Jahr. Geol. Bundes.* **1988**, *131*, 533–551.

138. Owen, J.P. Geochemistry of lamprophyres from the Western Alps, Italy: Implications for the origin of an enriched isotopic component in the Italian mantle. *Contrib. Miner. Petrol.* **2008**, *5*, 341–362. [CrossRef]

139. Callegari, E.; Cigolini, C.; Medeot, O.; D'Antonio, M. Petrogenesis of calc-alkaline and shoshonitic post-collisional Oligocene volcanics of the Cover Series of the Sesia Zone, Western Italian Alps. *Geodin. Acta* **2004**, *17*, 1–29. [CrossRef]

140. Lu, G.; Winkler, W.; Rahn, M.; von Quadt, A.; Willet, S.D. Evaluating igneous sources of the Taveyannaz formation in the Central Alps by detrital zircon U–Pb age dating and geochemistry. *Swiss J. Geosci.* **2018**, *111*, 399–416. [CrossRef]

141. Castro, A. On granitoid emplacement and related structures. A review. *Geol. Rundsch.* **1987**, *76*, 101–124. [CrossRef]

142. Brack, P. Muliple intrusions–examples from the Adamello batholith (Italy) and their significance on the mechanisms of intrusion. *Mem. Soc. Geol.* **1983**, *26*, 145–157.

143. John, B.E.; Blundy, J.D. Emplacement-related deformation of granitoid magmas, southern Adamello Massif, Italy. *Geol. Soc. Am. Bull.* **1993**, *105*, 1517–1541. [CrossRef]

144. Franzini, M.; Leoni, L.; Saitta, M. Revisione di una metodologia analitica per fluorescenza-X, basata sulla correzione completa degli effetti di matrice. *Rend. Soc. It. Mineral. Petrol.* **1975**, *31*, 365–378.

145. Leoni, L.; Saitta, M. X-ray fluorescence analysis of 29 trace elements in rock and mineral standards. *Rend. Soc. It. Mineral. Petrol.* **1976**, *32*, 497–510.

146. Alibert, C.; Michard, A.; Albarède, F. The transition from alkali basalts to kimberlites isotope and trace element evidence from melilitites. *Contrib. Mineral. Petrol.* **1983**, *82*, 176–186.

147. Clocchiatti, R.; Del Moro, A.; Gioncada, A.; Joron, J.L.; Mosbah, M.; Pinarelli, L.; Sbrana, A. Assessment of a shallow mag-matic system; the 1888–1890 eruption Volcano Island, Italy. *Bull. Volcanol.* **1994**, *56*, 466–486.

148. Palme, H.; O'Neill, H.S.C. Cosmochemical estimates of mantle composition. In *Treatise on Geochemistry, Vol. 3: The Mantleand Core*; Carlson, R.W., Ed.; Elsevier: New York, NY, USA, 2014; pp. 1–39.